Tectonics

RESEARCH ARTICLE
10.1029/2018TC004974

Key Points:
- Early Permian metamorphic core complex and extensional detachment fault are reconstructed in the Orobic Anticline (Southern Alps)
- Two synkinematic to postkinematic plutons in the metamorphic core complex are dated at ~289 and ~287 Ma by U-Pb LA-ICP-MS on zircon
- Early Permian tectonics represent N-S extension rather than dextral wrenching related to the Pangea B to A transformation

Supporting Information:
- Supporting Information S1

Correspondence to:
F. Pohl,
florian.pohl63@gmail.com

Citation:
Pohl, F., Froitzheim, N., Obermüller, G., Tomaschek, F., Schröder, O., Nagel, T. J., et al. (2018). Kinematics and age of syn-intrusive detachment faulting in the Southern Alps: Evidence for Early Permian crustal extension and implications for the Pangea A versus B controversy. *Tectonics*, *37*, 3668–3689. https://doi.org/10.1029/2018TC004974

Received 15 JAN 2018
Accepted 25 SEP 2018
Accepted article online 4 OCT 2018
Published online 15 OCT 2018

Kinematics and Age of Syn-Intrusive Detachment Faulting in the Southern Alps: Evidence for Early Permian Crustal Extension and Implications for the Pangea A Versus B Controversy

Florian Pohl[1,2], Nikolaus Froitzheim[2], Gerrit Obermüller[2], Frank Tomaschek[2], Oliver Schröder[2], Thorsten J. Nagel[3], Dario Sciunnach[4], and Alexander Heuser[5]

[1]Department of Earth Sciences, Utrecht University, Utrecht, Netherlands, [2]Steinmann Institute, Bonn University, Bonn, Germany, [3]Geology Department, University of Århus, Århus, Denmark, [4]Direzione Generale Ambiente e Clima, Regione Lombardia, Milan, Italy, [5]GEOMAR Helmholtz-Zentrum für Ozeanforschung, Kiel, Germany

Abstract Permian basin formation and magmatism in the Southern Alps of Italy have been interpreted as expressions of a WSW-ENE-trending, dextral megashear zone transforming Early Permian Pangea B into Late Permian Pangea A between ~285 and 265 Ma. In an alternative model, basin formation and magmatism resulted from N-S crustal extension. To characterize Permian tectonics, we studied the Grassi Detachment Fault, a low-angle extensional fault in the central Southern Alps. The footwall forms a metamorphic core complex affected by upward-increasing, top-to-the-southeast mylonitization. Two granitoid intrusions occur in the core complex, the synmylonitic Val Biandino Quartz Diorite and the postmylonitic Valle San Biagio Granite. U-Pb zircon dating yielded crystallization ages of 289.1 ± 4.5 Ma for the former and 286.8 ± 4.9 Ma for the latter. Consequently, detachment-related mylonitic shearing took place during the Early Permian and ended at ~288 Ma, but kinematically coherent brittle faulting continued. Considering 30° anticlockwise rotation of the Southern Alps since Early Permian, the extension direction of the Grassi Detachment Fault was originally ~N-S. Even though a dextral continental wrench system has long been regarded as a viable model at regional scale, the local kinematic evidence is inconsistent with this and, rather, supports N-S extensional tectonics. Based on a compilation of >200 U-Pb zircon ages, we discuss the evolution and tectonic framework of Late Carboniferous to Permian magmatism in the Alps.

1. Introduction

The Pangea B hypothesis, first formulated by Irving (1977), implies that the supercontinent Pangea underwent a fundamental geometric reorganization at the end of the Paleozoic era. According to this hypothesis, ~3,500-km dextral strike slip took place along a WSW-ENE-trending megashear between Pangea's northern part (Laurasia) and its southern part (Gondwana), transforming the Late Paleozoic Pangea B situation into the Mesozoic Pangea A situation (Irving, 1977). The hypothesis is based on paleomagnetic data, which imply a paleolatitudinal overlap of southern Laurasia and northern Gondwana during the Late Carboniferous and Early Permian. This overlap does not allow to place Laurasia entirely north of Gondwana, as in the Mesozoic Pangea A situation; instead, a part of Laurasia (i.e., southern North America) was located west of Gondwana (Figure 1). The Pangea B to A transformation, that is, the dextral displacement, was originally assumed to have taken place in the Triassic (Irving, 1977; Morel & Irving, 1981). Later, based on paleomagnetic data, from particularly the European Southern Alps, Muttoni et al. (1996, 2003) placed the transformation in the Permian at ~285–265 Ma. Such an Early to Middle Permian timing is now generally accepted among the proponents of the hypothesis (e.g., Gallo et al., 2017; Muttoni et al., 2009).

Other authors, however, have doubted the Pangea B hypothesis and proposed other explanations for the paleomagnetic data, like nondipole contributions to the Earth's magnetic field (Van der Voo & Torsvik, 2001) or systematic bias in the paleomagnetic data, for example, caused by sedimentary inclination shallowing (Domeier et al., 2012, and references therein). The controversy is not resolved (e.g., Gallo et al., 2017; Meijers et al., 2010). Like the paleomagnetic evidence, the geological record of the hypothetical megashear is controversial. Arthaud and Matte (1977) indeed reconstructed a Late Variscan dextral shear corridor in southern Europe and northern Africa. A through-going fault, however, was not identified but only

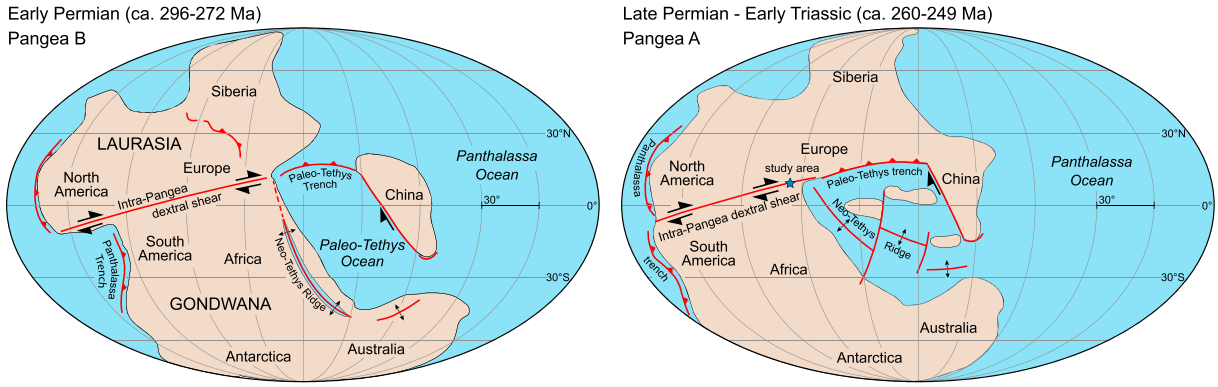

Figure 1. The transformation of Early Permian Pangea B to Late Permian-Early Triassic Pangea A by displacement along a dextral megashear (after Muttoni et al., 2009).

synthetic (dextral) and antithetic (sinistral) Riedel shears. The estimated total amount of displacement was only ~600 km instead of the required >3,000 km. Moreover, a substantial part of this displacement took place in the Late Carboniferous, that is, more than 15 Ma before the onset of the *paleomagnetic* Pangea A to B transformation as defined by Muttoni et al. (2003).

Permian Basins in the Southern Alps in Italy have played a prominent role in the Pangea A versus B controversy. Formed during a short period of time in the Early Permian and filled with thick clastic sediments and volcanic rocks, these basins have repeatedly been interpreted as dextral pull-apart basins (Cadel et al., 1996) within the Pangea A to B megashear and therefore as supporting evidence for the Pangea B hypothesis (Boriani et al., 2016; Muttoni et al., 2003, 2009; Schaltegger & Brack, 2007; Visonà et al., 2007). Other authors, however, interpreted them as products of crustal extension, unrelated to large-scale strike-slip (Marotta & Spalla, 2007; Schuster & Stüwe, 2008; Siletto et al., 1993; Spalla et al., 2014). In the present paper, we reconstruct the kinematics and timing of the Grassi Detachment Fault in the central Southern Alps of Italy, so far the Alps' only known Permian extensional detachment fault (Froitzheim et al., 2008). We report the results of geological field mapping and U-Pb zircon dating of syntectonic to posttectonic granitoids, to constrain the timing and kinematic framework of Early Permian magmatism and basin formation in this part of the Southern Alps. Based on these new results and on a compilation of published U-Pb zircon ages from Carboniferous and Permian magmatic rocks in the Alps, we then discuss the Permian tectonic framework of the Southern Alps and the Alpine region in general and the implications for the Pangea B hypothesis.

1.1. Permian Tectonics and Magmatism in the Southern Alps

The Southern Alps are an E-W-trending, south-vergent thrust belt, formed by Late Cretaceous to Neogene thrusting of the retrowedge of the Alps (see Zanchetta et al., 2015, for a review). The northern border is the Insubric Fault and the southern border the Po Basin (Figure 2). Compressional structures of the thrust belt reach into the subsurface of the Po Basin. The Southern Alps expose all levels of the continental crust of the Adria plate, from the crust-mantle boundary through middle and upper crustal basement to the post-Variscan sedimentary cover. This special situation results from uplift and tilting during Jurassic rifting and during the Alpine collisional orogeny (e.g., Beltrando et al., 2015; Bertotti, 1991; Real et al., 2018). It offers the rare possibility to study a magmatic system of Early Permian age through different structural levels, including magmatic underplating of gabbroic melt in the lower crust (Ivrea Zone: Rivalenti et al., 1984; Pin, 1986; Voshage et al., 1990), granitoid intrusions in the upper crust (e.g., Baveno: Pinarelli et al., 1988; Brixen: Del Moro & Visonà, 1982; Cima d'Asta: Borsi et al., 1974), and volcanic complexes associated with clastic sedimentary basins at the surface (e.g., Lugano-Valganna: Bakos et al., 1990; Orobic and Collio Basin: Sciunnach, 2001a; Cassinis et al., 2007; Athesian Volcanic Complex: Bargossi et al., 1998; localities in Figure 2). The timing of this magmatic activity is rather well constrained between 290 and 275 Ma (Schaltegger & Brack, 2007), but the tectonic framework is still unclear. Most authors have suggested that basin formation and volcanism were related to dextral strike slip along W-E to SW-NE striking faults (Cassinis et al., 2007, 2012; Gretter et al., 2013; Schaltegger & Brack, 2007; Stähle et al., 2001). In contrast, Handy et al. (1999) reconstructed transtension along WSW-ENE-striking sinistral strike-slip faults, that is, the opposite sense of shearing.

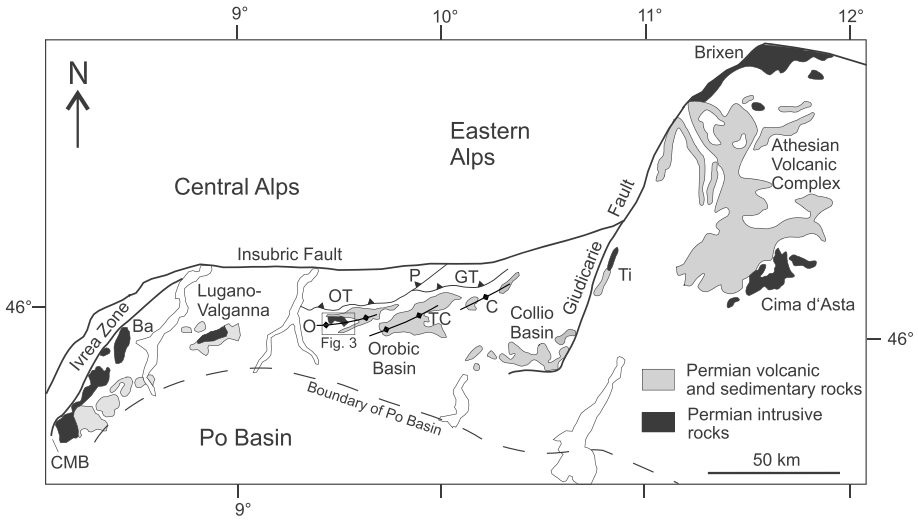

Figure 2. Distribution of Permian in the Southern Alps, modified after Cassinis et al. (2012). Lakes are indicated for orientation (from left to right: Lago Maggiore, Lago di Como, Lago d'Iseo, and Lago di Garda). Ba = Baveno granite, CMB = Cossato-Mergozzo-Brissago Fault, OT = Orobic Thrust, P = Porcile Line, GT = Gallinera Thrust, O = Orobic Anticline, TC = Trabuchello-Cabianca Anticline, C = Cedegolo Anticline, Ti = Tione Basin.

Direct kinematic analysis of Early Permian faults and shear zones is difficult because most Early Permian faults were later reactivated and overprinted by Mesozoic and/or Alpine deformation (e.g., Blom & Passchier, 1997). Some Alpine (Tertiary-age) faults, for example, the Giudicarie Fault (Figure 2), are interpreted as former Permian strike-slip faults (Cassinis et al., 2007) because they coincide with facies or thickness changes in the Permian basins. Due to strong Alpine overprint, Permian-age fault rocks are not preserved. Other faults, like the Cossato-Mergozzo-Brissago Line (CMB), that is, the southeastern border of the Ivrea Zone (Figure 2), contain Permian mylonites, but their kinematics are controversial. Handy et al. (1999) and Handy and Streit (1999) reconstructed the CMB as a sinistral, extensional, oblique-slip fault in the Early Permian. In contrast, Boriani et al. (2016) reconstructed transpressional, dextral kinematics for the Early Permian activity of the same shear zone. As compared to these examples, our study area is more suitable for a reconstruction of Permian tectonics because it is situated in the hinge of a gentle Alpine anticline, the Orobic Anticline. Alpine deformation is localized in fault systems north and south of the anticline, that is, the Orobic Thrust and the Valtorta Fault (Figure 3). The area in between stayed relatively unaffected by Alpine deformation except for gentle folding and local, minor thrusting.

1.2. Regional Geologic Setting

The study area is located in the Orobic Alps, which is the part of the Southern Alps between Lago di Como and Val Camonica, the valley extending from Lago d'Iseo toward northeast (Figure 2). The thrust sheets of the Orobic Alps are formed by Mesozoic marine carbonates in the southern part, and by pre-Mesozoic basement, partly with Permo-Carboniferous and Mesozoic cover, in the North. The Orobic Thrust (Figure 3) is the basal thrust of the uppermost thrust sheet which consists of Variscan basement, metamorphosed under amphibolite- to greenschist-facies conditions during the Variscan orogeny (Cadel et al., 1996; Diella et al., 1992; Milano et al., 1988; Mottana et al., 1985; Spalla et al., 2000). In our study area (Figure 3), the hanging wall of the Orobic Thrust is formed by Gneiss Chiari del Corno Stella, Variscan amphibolite-facies orthogneisses formed from Ordovician granitoid protoliths (Boriani & Bini, 2012). A Late Cretaceous age is inferred for the Orobic Thrust (Zanchetta et al., 2015). In the footwall, several anticlines are present, which expose basement and Permian rocks, surrounded by Mesozoic sedimentary rocks. The anticlines are interpreted as fault-bend folds (Laubscher, 1985; Schönborn, 1990, 1992), formed by southward thrusting during the Eocene (Zanchetta et al., 2015). The westernmost of these is the Orobic Anticline. It exposes Variscan basement, the Morbegno Gneiss (Cornelius, 1916), in its core (Figures 3 and 4). The Morbegno Gneiss is intruded by two plutons, the Val Biandino Quartz Diorite (VBQD; Pasquaré, 1967) and the Valle San Biagio Granite (VSBG; Porro, 1897; De Sitter & De Sitter-Koomans,

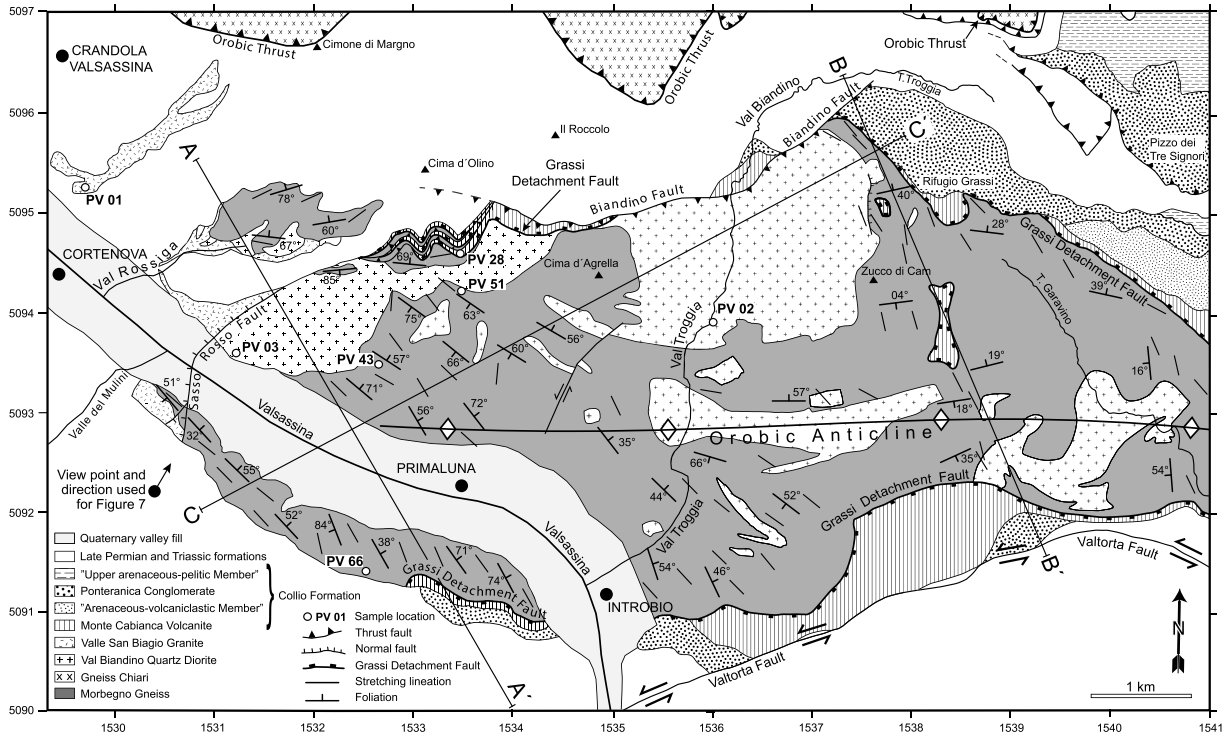

Figure 3. Geological map of the study area including the position of the samples used for this study and representative foliation and stretching lineation measurements. Cross sections A-A′, B-B′, and C-C′ are shown in Figure 4. Grid: UTM Universal Transverse Mercator, Zone T32, WGS 84.

1949; Figures 3 and 4). The age of the VBQD is poorly constrained at 312 ± 48 Ma by Rb-Sr whole-rock dating (Thöni et al., 1992). The VSBG has not yet been dated, but geometric relations suggest an Early Permian age for this intrusion (Gaetani et al., 2012).

The Variscan basement including the two intrusions is overlain by up to 1,250-m-thick volcanic and sedimentary rocks of the Early Permian Collio Formation (Sciunnach, 2001a). The stratigraphic terminology has recently been revised and *Collio Formation* has been replaced by different names for different basins (see Berra et al., 2016; Gaetani et al., 2012); however, we will use the old term for simplicity. The Collio Formation was deposited in two basins (or subbasins of one large basin), the Orobic Basin, including our study area, and the Collio Basin further southeast (Figure 2). The Collio Formation is subdivided into volcanic rocks at the base (Monte Cabianca Volcanite) and a sedimentary succession with intercalated volcanic rocks at the top (Pizzo del Diavolo Formation). The volcanic rocks at the base comprise welded tuffs, lapillistones, porphyric ignimbrites, massive volcanites, and volcanic breccias that can be classified as benmoreites to rhyodacites based on geochemistry (Sciunnach, 2003, and references therein). The sedimentary succession (Pizzo del Diavolo Formation) comprises in the area of the Orobic Anticline (from base to top) the *arenaceous-volcaniclastic member*, the Ponteranica Conglomerate, and the *upper arenaceous-pelitic member* (Sciunnach, 2001a). The Collio sediments were generally deposited in an alluvial to lacustrine environment in fault-controlled basins (Sciunnach, 2001a, 2001b) but rare benthic foraminifera in the uppermost part record a marine ingression (Sciunnach, 2001c).

U-Pb zircon ages for volcanic rocks of the Collio Formation range from ~287 to ~270 Ma (Berra et al., 2015; Cadel, 1986; Philippe et al., 1987; Schaltegger & Brack, 2007). However, Berra et al. (2015) also found a ~291-Ma zircon population, interpreted as antecrystic zircons, in basal volcanics of the Collio Formation. The youngest ages around 270 Ma are controversially discussed; most authors assume that the deposition of the Collio Formation ended by ~278 Ma (e.g., Cassinis et al., 2012). In the western part of the Orobic Anticline, the contact between the Collio Formation and the underlying Variscan basement is marked by a layer of cataclasite and underlain by mylonites. This contact represents a detachment fault, the Grassi Detachment (Froitzheim et al., 2008), as will be discussed in detail below.

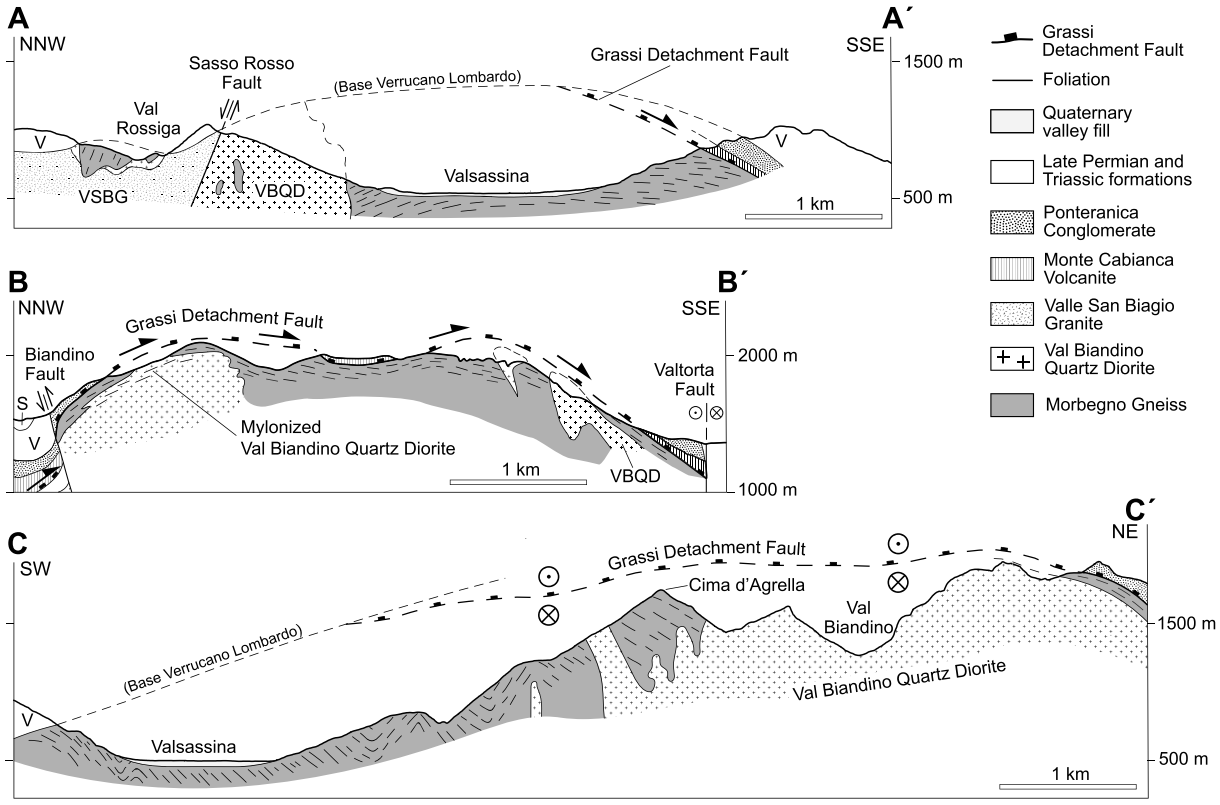

Figure 4. Cross sections of the Orobic Anticline in the study area (see Figure 3 for traces). Cross section A-A′ is parallel to the displacement direction of the Grassi Detachment. The Grassi Detachment in the SSE part of the section, and the Sasso Rosso Fault in the NNW are both sealed by the erosional base of the Verrucano Lombardo Formation. Section B-B′ shows the Grassi Detachment Fault overlain by allochthonous Collio Formation. Foliation in the mylonites below the Grassi Detachment is subparallel to the detachment itself. Section C-C′ is perpendicular to the movement direction of the Grassi Detachment Fault and shows the D3 folds in the Morbegno Gneiss representing extension-parallel corrugation folds. Abbreviations: V = Verrucano Lombardo Formation, S = Servino Formation.

The Collio Formation is overlain by the Middle (?) to Late Permian (Gaetani et al., 2012) Verrucano Lombardo Formation of fluvial conglomerates and sandstones. The thickness of this formation increases from west (<100 m) to east (>400 m) in the area shown in Figure 3 (Sciunnach, 2001b). The contact with the underlying rocks (either Collio Formation or basement) is erosive and unconformable (Casati & Gnaccolini, 1967). In the westernmost part of the Orobic Anticline (west of grid line 1533; Figure 3), the Verrucano Lombardo Formation lies directly on the Variscan basement and Permian intrusions (VBQD and VSBG). Deposition of the Verrucano Lombardo started in the Orobic Alps at ~260 Ma (Cassinis et al., 2012). The Verrucano Lombardo Formation is overlain by the Servino Formation, siliciclastic to carbonatic sedimentary rocks of Early Triassic age (Gaetani et al., 2012). Various carbonatic rocks of Middle Triassic age follow stratigraphically - up-section.

2. Basement Rocks and Their Structural Relations

2.1. Morbegno Gneiss

The Morbegno Gneiss is the most common and oldest rock type in the core of the Orobic Anticline. It comprises dark gray, banded paragneisses, mica schists, and mica-bearing quartzites with intercalated layers of amphibole-bearing gneiss and amphibolite. In the paragneiss, the peak equilibrium phase assemblage comprises quartz, biotite, plagioclase, white mica, garnet, staurolite, and kyanite, reflecting amphibolite-facies conditions reached during the Carboniferous (between 350 and 315 Ma; Boriani et al., 1985). Chlorite, epidote/clinozoisite, stilpnomelane, and sericite are products of retrograde metamorphism.

The main foliation, formed during the second deformation phase (D2), is defined by dark layers rich in biotite and/or chlorite and light-colored layers rich in quartz and feldspar. Isolated, isoclinal fold hinges are relicts of

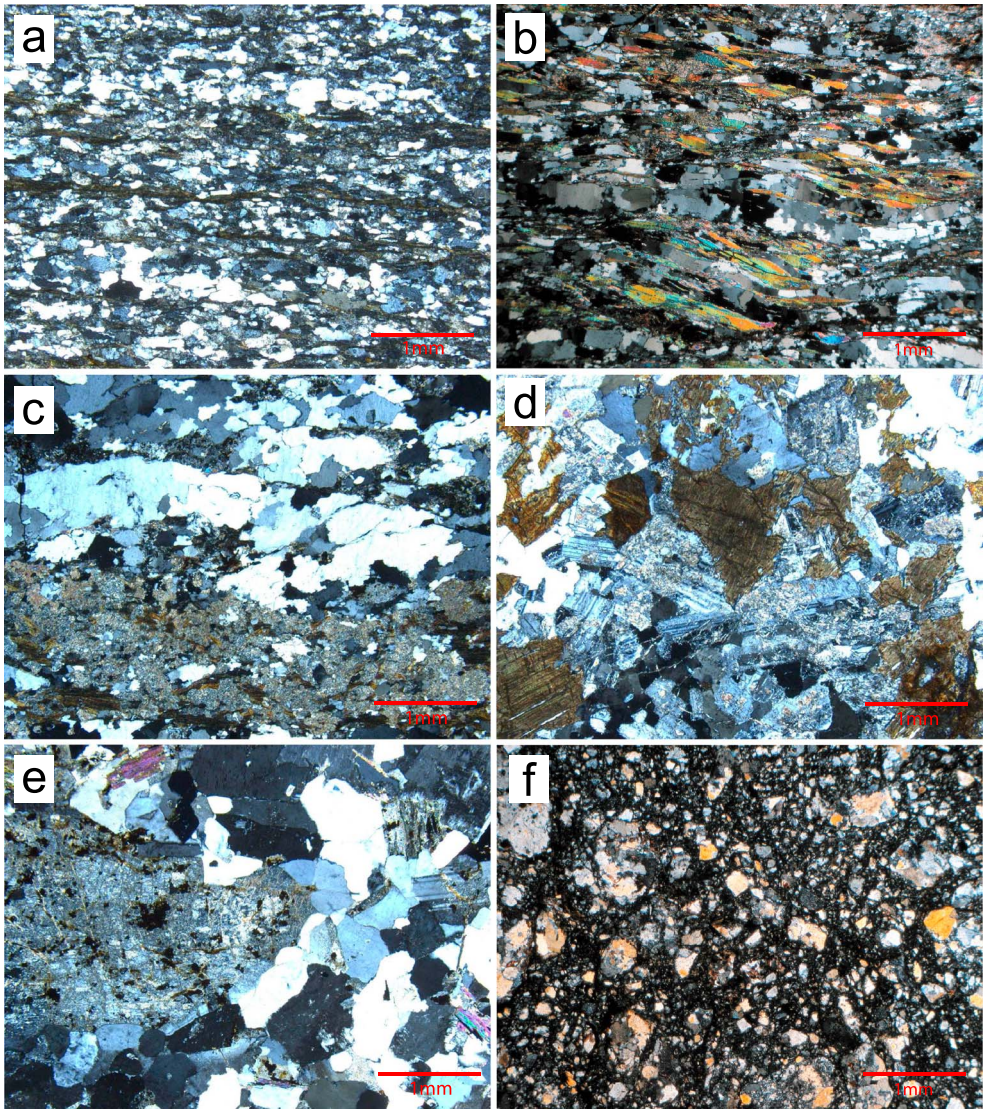

Figure 5. Thin-section photographs of rocks from the footwall of the Grassi Detachment Fault. (a) Sample PV51. Mylonitized Morbegno Gneiss close to the detachment showing a well-developed foliation. Bright layers are recrystallized quartz, dark layers are rich in biotite. (b) Sample PV66. Morbegno Gneiss close to the Grassi Detachment Fault with shear bands indicating a sinistral (top-to-the-southeast) shear sense. (c) Sample PV43. Weakly mylonitized Morbegno Gneiss located approx. 250 m below the detachment. Note larger grain size than in (a) and (b). (d) Sample PV02. Val Biandino Quartz Diorite containing plagioclase, quartz, and biotite. Plagioclase is partly replaced by sericite and biotite by chlorite. (e) Sample PV01. Valle San Biagio Granite. On the left side of the image, a K-feldspar phenocryst is partly replaced by sericite. (f) Sample PV28. Cataclasite from the Grassi Detachment Fault. See Figure 3 for sample locations. All images are in cross-polarized light.

an earlier deformation phase (D1). These formed under peak amphibolite-facies conditions and were strongly overprinted by the main foliation afterward (Gaetani et al., 2012; Siletto et al., 1993). In most places, a stretching lineation is visible on the foliation. It is generally oriented NW-SE (Figure 3), with a maximum at 333°/11° (plunge direction/plunge). In sections perpendicular to the foliation and parallel to the stretching lineation, the rock shows mylonitic structure: dynamic recrystallization of quartz and formation of quartz ribbons, shear bands in mica-rich layers, mica fishes, and plagioclase and garnet porphyroclast systems (Figures 5a and 5b). The intensity of mylonitization increases upward and reaches a maximum at the top of the Morbegno Gneiss. This is shown by upward-decreasing grain size of all minerals and decreasing spacing of the foliation planes (Figures 5a and 5c). At deeper structural levels, that is, more than ~50 to 100 m below the structural top of the basement, and in the vicinity of the VBQD intrusions, biotite is a

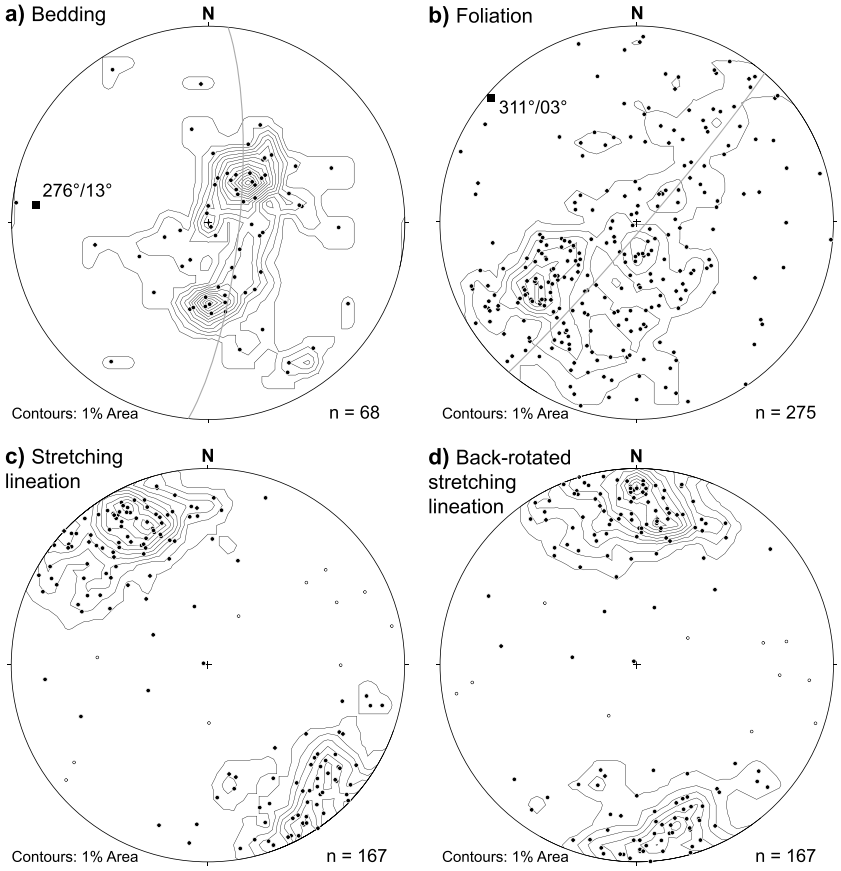

Figure 6. Schmidt nets of structural elements from the study area (lower hemisphere). (a) Poles to bedding of the sedimentary rocks in the Orobic Anticline. Best cylindrical fit of the data yields a shallowly west-dipping fold axis related to Alpine tectonics, that is, formation of the Orobic Anticline, oriented 276°/13° (plunge direction/plunge). (b) Poles to foliation of the Morbegno Gneiss in the core of the Orobic Anticline. Best cylindrical fit of the data yields a subhorizontal fold axis oriented 311°/03°, related to D3 folding. (c) Stretching lineations of the Morbegno Gneiss. Open circles are measurements northwest of the Sasso Rosso Fault, not considered for the calculation of the contours. Predominant orientation of the stretching lineation is northwest-southeast with a maximum at 333°/11°. (d) Stretching lineations of the Morbegno Gneiss back-rotated by 30° clockwise to restore the Early Permian situation. Extension direction was N-S. Measurements are shown in Table S8 of the supporting information.

stable synkinematic phase during D2, together with white mica. Distant from the intrusions and near the top of the basement, however, biotite has been partly or completely replaced by chlorite during the mylonitization (see Figure 6 in Froitzheim et al., 2008). Shear-sense indicators, including asymmetric porphyroclast systems, shear bands, mica fishes, and shape- and crystallographic preferred orientation in quartz, consistently show top-to-the-Southeast transport (Figure 5b and Froitzheim et al., 2008).

In the small outcrop area of Morbegno Gneiss northwest of the Sasso Rosso Fault (Figures 3 and 4, profile A-A′), the rock does not show evidence of mylonitic shearing, but rather a normal gneissic structure and biotite are preserved. The foliation dips steeply north to northwest and a W-E- to SW-NE-oriented mineral lineation is visible in some places. We interpret the structures in this area as D1.

East of the Sasso Rosso Fault, the main foliation (D2) is folded around upright, open to tight D3 folds with NW-SE axes. In Schmidt projection (Figure 6b), the girdle distribution of D2 foliation poles from the entire area east of the Sasso Rosso Fault indicates a fold-axis orientation of 311°/03° (plunge direction/plunge). Hence, the D3 fold axes are subparallel to the D2 stretching lineation. West of Val Troggia, the D3 folds are quite pronounced and have steep limbs with dip angles up to >70° (Figures 3 and 4, profile C-C′). Crenulation cleavage is associated with the folds, the crenulation axes (D3) being parallel or subparallel to the stretching lineation (D2). From Val Troggia toward east, the D3 folds become gentler; in the area of Rifugio Grassi and Zucco di Cam (Figure 3), there are hardly any D3 folds, and the D2 foliation is parallel to the top of the basement.

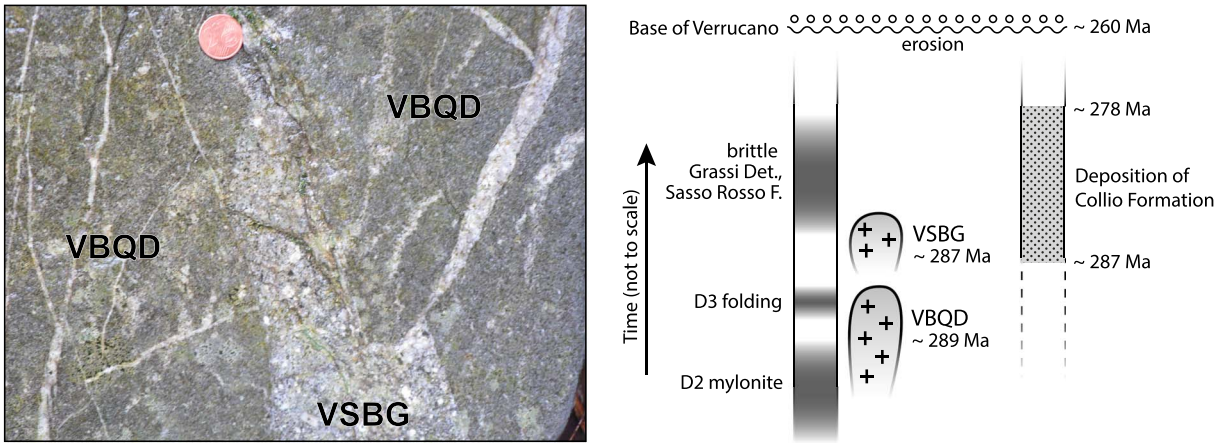

Figure 7. Overprinting relations in the study area. Left: Contact zone between Val Biandino Quartz Diorite (VBQD) and Valle San Biagio Granite (VSBG), Val Rossiga NE of Cortenova. Fractures across VBQD are filled with VSBG. Right: Geohistory diagram. Ages of VBQD and VSBG from this study; ages at the right column after Cassinis et al. (2012).

On the southern side of Valsassina, D3 folds are truncated by the erosive base of the Verrucano Lombardo (Figure 3: southwest of Primaluna).

2.2. Val Biandino Quartz Diorite

The VBQD intruded the Morbegno Gneiss forming several irregularly shaped stocks, lenses, and dykes. The predominant rock type is quartz diorite comprising quartz, plagioclase, and biotite as major constituents and amphibole, K-feldspar, and zircon as minor phases. Due to alteration, plagioclase is partly replaced by sericite and biotite by chlorite. Whereas east of Val Troggia, the quartz diorite has locally been mylonitized during D2 (near Rifugio Grassi, Figure 8 in Froitzheim et al., 2008), it shows only slight deformation, for example, kinking of biotite, to the West (Figure 5d).

Other rock types included in the VBQD are high-K tonalites, gabbrodiorites, and aplitic granites (De Capitani & Liborio, 1988; Pasquaré, 1967; Thöni et al., 1992). This results in a broad variation of color, composition, and fabric. De Capitani and Liborio (1988) suggest that all the different magma compositions had the same origin. They infer that a dioritic magma stagnated in a magma chamber near the crust-mantle boundary from where pulses of magma went up to ~10–12-km depth (depth of intrusion). These incorporated crustal material, resulting in the different compositions. Cordierite, andalusite, and sillimanite occur in the Morbegno Gneiss in contact metamorphic aureoles of the VBQD (Gaetani et al., 2012; Pasquaré, 1967).

K-Ar biotite ages of ~300 Ma for the quartz diorites and ~291 to 294 Ma for the granitoid compositions of the VBQD were reported by De Capitani and Liborio (1988) and De Capitani et al. (1988). Rb-Sr whole rock analysis by Thöni et al. (1992) on quartz diorites and granites yielded an age of 312 ± 48 Ma. Using only the analyses from granitic rocks resulted in an age of 286 ± 20 Ma.

2.3. Valle San Biagio Granite

The VSBG is exposed in the westernmost part of the Orobic Anticline. It is a porphyric leucogranite with pinkish K-feldspar phenocrysts up to 1 cm in size. The phenocrysts are subhedral, typically altered and partly replaced by sericite (Figure 5e). The holocrystalline matrix is mainly formed by K-feldspar, plagioclase, and quartz. Plagioclase is partly replaced by sericite. Minor constituents are biotite, apatite, rutile, tourmaline, allanite, and zircon. Locally, the VSBG shows zones with a fine-grained, granophyric structure (Gaetani et al., 2012; Sciunnach, 2001b). These are of metric size and separated from the porphyric zones by sharp boundaries. In a small area west of the Sasso Rosso Fault, VSBG is in contact with VBQD (Figure 3). Near the contact, fractures in the VBQD are filled by VSBG (Figure 7), showing that VSBG is younger than VBQD.

As already noted by Porro (1897) and Merla (1933), the VSBG shows petrological analogies with the Early Permian Monte Cabianca Volcanite at the base of the Collio Formation, suggesting that the granite is the magma chamber from which the latter was fed. The occurrence of granophyric structure suggests that the VSBG intruded at a considerably shallower depth than the VBQD.

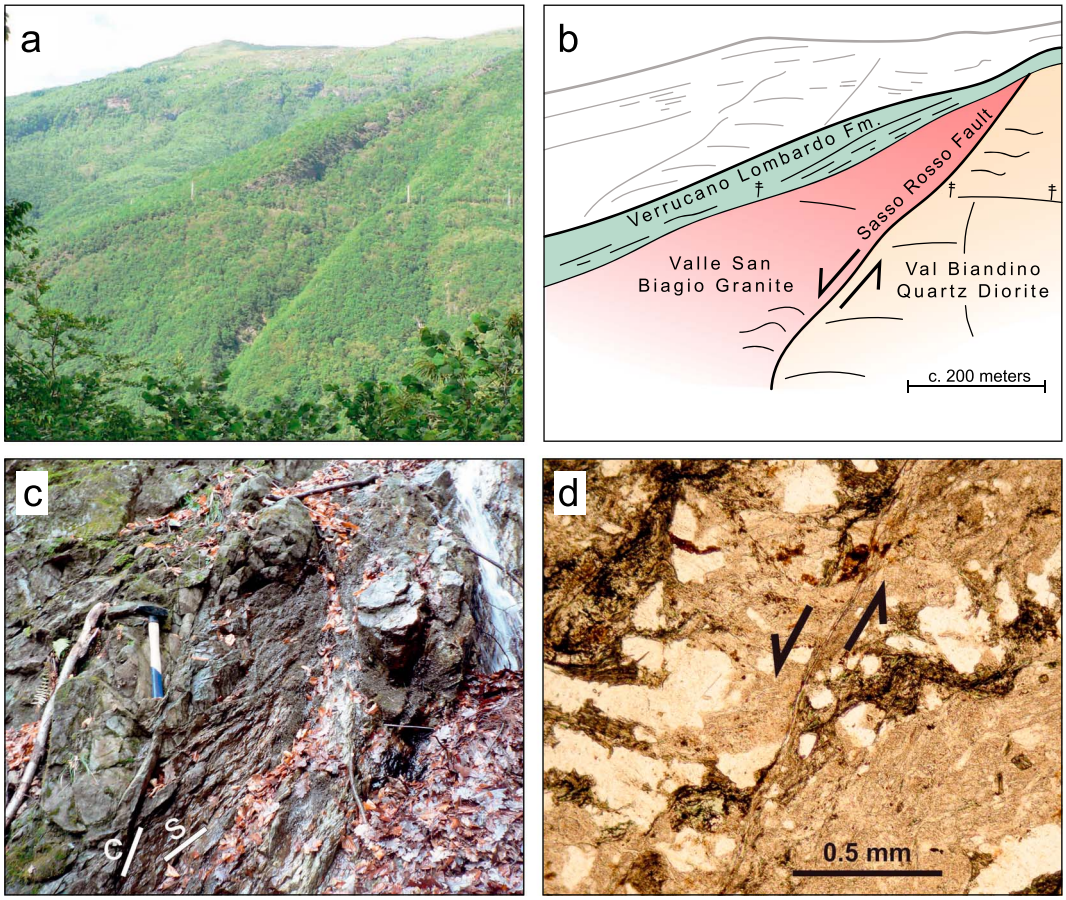

Figure 8. (a, b) Bosco di Sasso Rosso, seen from the South-Southwest (see Figure 3 for location). The Sasso Rosso Fault, a normal fault dipping approximately 70° to the northwest, separates Valle San Biagio Granite in the hanging wall from Val Biandino Quartz Diorite in the footwall and is sealed by Late Permian Verrucano Lombardo, indicating pre-Late-Permian faulting. (c) Foliated cataclasite along the Sasso Rosso Fault with S-C structure indicating top-NW normal fault displacement (NW is to the left). Length of hammer: 36 cm. (d) Thin-section photograph of the cataclasite with foliation marked by dark green chlorite and shear band by arrows. Plane-polarized light; same orientation as in (c).

2.4. Grassi Detachment Fault, Sasso Rosso Fault, and Related Cataclasites

Everywhere in the Orobic Anticline, the basement is separated from the overlying Collio Formation by a cataclasite layer up to 4 m thick and black to dark ochre in color (Figure 5f). It consists of clay minerals, fragments of quartz-feldspar-dominated, altered rocks, and secondary ankerite. The cataclasite represents the Grassi Detachment Fault (Froitzheim et al., 2008). East of Val Troggia, it is approximately concordant with the underlying mylonites, and a transition between mylonite and cataclasite can be observed, but further west, the cataclasite layer becomes discordant to the mylonitic foliation, for example, south of Primaluna where the cataclasite dips shallowly south whereas the underlying mylonites dip steeply northeast (Figure 3). This transition from concordant to discordant relations accompanies the westward intensification of D3 folding and is the result of it. Southwest of Primaluna, the cataclasite layer is unconformably sealed by the basal sediments of the Verrucano Lombardo (Figures 3 and 4, profile A-A′), indicating that the cataclasite layer is older than Late Permian. Conversely, near Cima d'Olino the cataclasite is involved in a small-scale, south-vergent, Alpine thrust duplex that makes Alpine reactivation of the cataclasite very likely. Therefore, we were not able to unambiguously relate small-scale structures in the cataclasite to either pre-Alpine or Alpine deformation and do not present such data here.

The contact between the VBQD and the VSBG is formed by a steeply (~70°) northwest-dipping fault between Primaluna and Cortenova (Figures 3 and 4, profile A-A′). This fault was identified as a Permian palaeofault, the *Cortabbio/Cortenova boundary fault system* by Sciunnach (2001b, 2003). We call it Sasso Rosso Fault since it crops out in Bosco di Sasso Rosso (Red Stone Wood), aptly named after the red cliffs of Verrucano

Lombardo conglomerates (Figures 8a and 8b). The unconformable base of the Verrucano Lombardo seals the fault and constrains its age to be older than Late Permian. Conversely, the fault is younger than the VSBG, forming the hanging wall, and the VBQD in the footwall. Both are brittlely deformed along the fault and transformed into a layer of black, partly foliated cataclasite with tourmaline mineralization (Sciunnach, 2001b). Slickenside lineations in the cataclasite plunge west to northwest (azimuth between 278° and 316°). S-C fabric indicates normal-fault relative movement at outcrop scale (Figure 8c) and thin section scale (Figure 8d). On the other (southwestern) side of Valsassina, the footwall of the Sasso Rosso Fault is formed by mylonitic Morbegno Gneiss and the hanging wall by VSBG and Morbegno Gneiss (Figure 3). Northwest of the Sasso Rosso fault, in the northwest corner of the map (Figure 3), Morbegno Gneiss, VSBG, and VBQD crop out in two tributary valleys. The outcrop pattern in the southern of the two valleys shows patches of VBQD between the Morbegno Gneiss and the VSBG (Figures 3 and 4, profile A-A′). As mentioned above, the Morbegno Gneiss in this area shows only D1 fabric. The D2 mylonites, which are predominant southeast of the Sasso Rosso Fault, do not occur here. We interpret that their continuation is below the outcrop level because they have been downthrown by the Sasso Rosso Fault.

2.5. Alpine Deformation

The Alpine deformation of the core of the Orobic Anticline is rather gentle and left the Permian structure almost in its original geometry. The Schmidt net of the poles to bedding of the sedimentary formations (Figure 6a) shows a girdle distribution indicating a fold axis plunging shallow west (plunge direction/plunge: 276°/13°). This is the orientation of the axis of the Orobic Anticline. The westward plunge of the axis is reflected in map view by the closure of the anticline at the western end of the study area (Figure 3). Most bedding planes dip rather gently, forming two maxima in the Schmidt net representing the two flanks of the anticline. Therefore, it can be assumed that the outcrops of Morbegno Gneiss in the core of the Orobic Anticline have only moderately been deformed and reoriented by the Alpine shortening, with the exception of the abovementioned minor south-directed thrusts that overprinted the Grassi Detachment at Cima d'Olino north of Primaluna, and the Biandino Fault, a steeply south-dipping backthrust cutting the northern flank of the Orobic Anticline between Cima d'Olino in the West and Val Biandino in the East (Figure 3).

2.6. Age Relations Between Deformation Structures, Intrusions, and the Collio Formation

Evidence for synmylonitic intrusion of the VBQD mainly comes from the area east of Val Troggia and was documented in Froitzheim et al. (2008). The following observations are critical: (1) Quartz textures from samples of mylonitized Morbegno Gneiss indicate that temperatures during D2 deformation were higher in the vicinity of the VBQD intrusions than distant from the intrusions; (2) in mylonites in the vicinity of the intrusions, red-brown biotite is stable during mylonitization; away from the VBQD, chlorite is stable, again indicating different temperatures during deformation; (3) VBQD has locally been mylonitized during D2, with the same kinematics as the Morbegno Gneiss; (4) locally, undeformed VBQD contains xenoliths of mylonitic Morbegno Gneiss. Observations (1) and (2) show that the VBQD intrusions were heating up their surroundings during D2 deformation, (3) shows that some of the D2 shearing postdated some of the VBQD intrusion, and (4) shows that some of the VBQD intrusion postdated some of the D2 shearing. Taken together, this shows that D2 mylonitic shearing and the different pulses of VBQD intrusion are roughly coeval. The VBQD body northwest of Primaluna (Figure 3) also truncates D3 folds, indicating that VBQD intrusion continued during D3. The VSBG does not show evidence for syn-D2 intrusion; it is generally undeformed, except for brittle deformation (cataclasite) along the Sasso Rosso Fault.

The brittle Grassi Detachment Fault, that is, the cataclasite layer, must be younger than the D2 mylonites and also younger than the D3 folding of these mylonites because D3 folds are truncated by the detachment fault southwest of Primaluna. It is younger than the VBQD because it truncates this intrusion north of Cima d'Agrella. The brittle Grassi Detachment Fault is also younger than the Monte Cabianca Volcanite, *Arenaceous-volcaniclastic member*, and Ponteranica Conglomerate of the Collio Formation in its hanging wall, since it cuts these units and the contacts between them (Figure 3). Conversely, it is older than Verrucano Lombardo because it is unconformably sealed by these sediments southwest of Primaluna. The Sasso Rosso Fault must be younger than both VBQD and VSBG because it cuts through these intrusions and older than the Verrucano Lombardo because it is sealed by it on both sides of Valsassina (Figure 8).

3. U-Pb Zircon Dating

Two characteristic samples of the intrusive rocks were dated. Sample PV01 is a VSBG from the type locality, Valle San Biagio north of Cortenova. Sample PV02 is a VBQD from the largest stock of quartz diorite in Val Troggia. The sampling localities are indicated in Figure 3; the sample coordinates are 1529552 East, 5095390 North (UTM Zone T32) for PV01 and 1535945 East, 5093886 North for PV02. The chemical compositions are indicated in Table S1 of the supporting information. Thin-section photographs of the two samples are shown in Figures 5d and 5e.

3.1. Methods

U-Pb zircon geochronology via laser ablation inductively coupled mass spectrometry was performed on zircon from the VBQD (Sample PV02) and the VSBG (Sample PV01). All analyses were conducted at Steinmann Institute, Bonn. The samples were crushed, milled, and sieved. Appropriate grain sizes of 63–250 μm underwent further magnetic and heavy liquid separation. Mostly optically clear, unaltered crystals without cracks or inclusions were handpicked under a binocular microscope and then mounted in epoxy resin and polished to half section. Cathodoluminescence imaging was performed on the JEOL 8200 Superprobe to reveal internal zoning and structures of all zircon crystals individually.

Laser ablation inductively coupled mass spectrometry analyses were carried out using a Resonetics RESOlution M50-E 193 nm excimer-laser coupled to a Thermo Scientific ELEMENT XR SF-ICP-MS. U-Pb data for zircon was collected following an adaption of methods previously used in our lab (Nilius et al., 2016). Material was ablated for 30 s with a laser spot size of 33 μm (44 μm) at 8 Hz and a fluency of ~7 J/cm^2. To avoid surface contamination, each spot was precleaned by three shots at an enlarged diameter followed by a 60-s wash out. A detailed list of analytical strategy and instrument settings for zircon analyses can be found in the supporting information Table S2. Downhole fractionation as well as mass bias and instrument drift were normalized to the 91500 zircon (Wiedenbeck et al., 1995, 2004), and Plešovice zircon (Sláma et al., 2008) was measured to estimate the systematic error and guarantee accuracy (supporting information Table S3; Figure 1). The acquired raw data were processed using the VizualAge (2015.06) data reduction scheme in Iolite 2.5 (Paton et al., 2011; Petrus & Kamber, 2012). All age calculation and plotting of data were done using the Isoplot Excel add-in (Ludwig, 2012). A systematic error of 1.5% was propagated by quadratic addition into the final age of the unknown populations.

3.2. Results

The zircons are optically clear, colorless, and mostly free of cracks and inclusions. They typically range from 50 to rarely 150 μm in size and have sub-equant to slightly elongated prismatic habit with width-to-length ratios of 1:1 to 1:2. Occasionally, elongated prismatic grains show a width-to-length ratio of up to 1:3 with a long axis of up to 250 μm. CL imaging (supporting information Figure S2) revealed an internal structure dominated by oscillatory zoning patterns that typically indicate magmatic growth of the mineral (Corfu et al., 2003). Some zircons show irregular structures that do not seem to yield different ages than the predominant zoning pattern. Zircons of the VBQD (PV02) have U contents between 124 and 598 ppm and Th-U ratios between 0.5 and 1.1. The VSBG (PV01) zircons show U contents between 117 and 1292 ppm. Th-U ratios are between 0.2 and 1.6. Due to the small size of most zircons, many analyses had to be disregarded when the laser spot was partially located in epoxy resin or when the interval times due to cracks, inclusions, or too little depth of the zircon grains were too short to give reliable results (i.e., under 8 s). Discordant analyses due to lead loss or a common lead component have been excluded from the age calculation. Furthermore, the data for the VSBG (PV01) contains three analyses with an average age of around 770 Ma. These represent inherited zircons and have been disregarded as well.

Results of the U-Pb analyses are shown in Figure 9a and in the supporting information Table S4 for the VBQD (PV02) and Figure 9b and in the supporting information Table S5 for the VSBG (PV01). Zircons of the VBQD (PV02) yielded single-spot $^{206}Pb/^{238}U$ ages between 277 and 306 Ma. A concordia age of 289.1 ± 1.2 Ma (internal error) was calculated with a low probability of 0.093. Therefore, the TuffZirc algorithm of Ludwig and Mundil (2002) was also applied resulting in a population of 36 zircons giving a $^{206}Pb/^{238}U$ age of 289.1 + 1.0/−1.5 Ma (internal error), which by quadratic addition of a systematic error of 1.5% results in an absolute age of 289.1 + 4.4/−4.6 Ma (internal and external error). The VSBG (PV01) single spot $^{206}Pb/^{238}U$ ages vary from 270 to 295 Ma. The concordia age of 287.8 ± 1.2 Ma (internal error) has a probability of

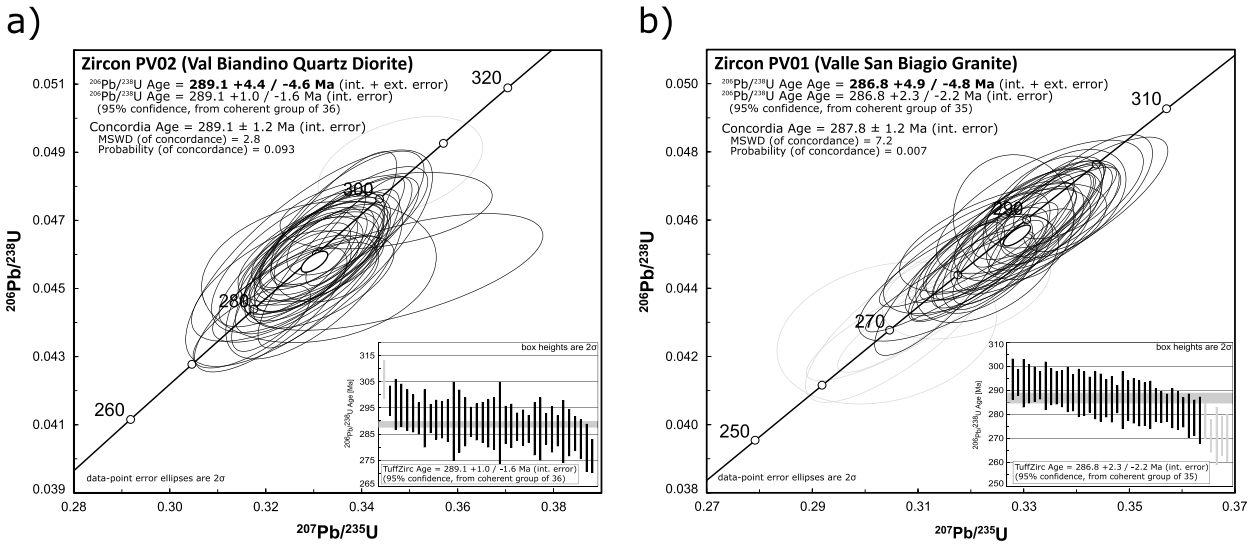

Figure 9. (a, b) Concordia diagrams for laser ablation inductively coupled mass spectrometry measurements of zircon. Analyses marked in black were used for the TuffZirc age calculation, gray analyses were rejected (inset). All ages are given with an internal error and with an additional external error of 1.5% propagated by quadratic addition. MSWD = Mean Square of Weighted Deviated.

0.007. Application of the TuffZirc algorithm yielded a $^{206}Pb/^{238}U$ age of 286.8 + 2.3/−2.2 Ma (internal error) from a coherent group of 35 analyses. Including a systematic error of 1.5% propagated by quadratic addition, this yields an absolute age of 286.8 + 4.9/−4.8 Ma (internal & external error). The ages for both samples are identical within error.

4. Hornblende Barometry

The composition of magmatic hornblende was studied to constrain the depth of crystallization of the VBQD. The measurements were made on a JEOL Superprobe JXA 8200 at Steinmann Institute, Bonn, with an acceleration voltage of 15 kV and a current of 15 nA. The results are shown in Table 6 of the supporting information. Due to low-grade metamorphic overprint, most samples only contain altered amphibole remnants. Unaltered magmatic hornblende was identified in two samples, PV02 and PV03. PV02 comes from Val Troggia and PV03 from Valsassina, a short distance east of the Sasso Rosso Fault (Figure 3). Both samples contain the assemblage generally used for hornblende barometry (Hammarstrom & Zen, 1986; Mutch et al., 2016; Schmidt, 1992): plagioclase, hornblende, biotite, K-feldspar, quartz, sphene, and Fe-Ti oxides. In PV02, calculated pressures range between 1.72 and 2.40 kbar in 12 measurements following the calibration of Mutch et al. (2016). The average pressure of the main population is 2.20 kbar with ±0.05 kbar as a 1-sigma standard deviation of the measured population (the error of derived pressure using the calibration of Mutch et al., 2016, is about ±16%). The obtained pressure is equivalent to a crystallization depth of 8.3 km assuming lithostatic pressure and a density of 2,700 kg/m^3 for the overlying rocks. In PV03, 13 analyses of the dominant hornblende generation yielded pressures between 1.46 and 2.26 kbar with an average of 1.97 kbar (±0.09) or 7.3-km depth. Additionally, a distinct older hornblende generation with considerably higher Al contents exists in PV03. Six analyses of this generation yielded pressures of 3.31 to 4.07 kbar, with an average of 3.64 kbar (±0.13 kbar), equivalent to a depth of 13.8 km.

5. Discussion

5.1. Age of Intrusions

Zircon dating yielded 289.1 ± 4.5 Ma for the VBQD and 286.8 ± 4.9 for the VSBG. Field relations show that the VBQD is older (Figure 7) but the age difference is not sufficient to be resolved by our dating. Both intrusions thus formed in the typical time span of Early Permian magmatism in the Southern Alps (e.g., Schaltegger & Brack, 2007) and the Austroalpine (Petri et al., 2017). The age of the basal volcanites of the Collio Formation (Monte Cabianca Volcanite), ~287 to ~278 Ma (Berra et al., 2015; Cadel, 1986; Philippe et al.,

1987), overlaps with the age of the intrusions. This supports a genetic link between the intrusions and these volcanites. In particular, the VSBG may represent part of the plumbing system from through which the geochemically similar volcanites were fed. The ~291-Ma antecrystic zircon population in the basal volcanics of the Collio Formation (Berra et al., 2015) is also compatible with these data. These zircons may have been derived from the VBQD magma chamber.

5.2. Intrusion Depth

Although the data are very limited, they allow some inferences that accord well with the model of intrusion in an evolving metamorphic core complex. In both samples, the dominant hornblende generation can be assumed to have grown during the final crystallization of the quartz diorite, at a depth of ~7 km for PV03 and ~8 km for PV02. Scatter in the data might well reflect continuous crystallization during exhumation; hence, these depths should not be viewed as a *static* intrusion depth. Both samples lie structurally 0.5 to 1 km below the Grassi Detachment (Figures 3 and 4). Their paleodepth after the end of detachment faulting was not more than 1 to 1.5 km since the thickness of the Collio Formation overlying the detachment is less than 500 m in this area. Consequently, PV02 was exhumed by ~6.5 km after its main crystallization and PV03 by ~5.5 km. This exhumation was the result of unroofing by the brittle Grassi Detachment Fault. The slightly greater amount of exhumation for PV02 conforms well with the position of this sample more downdip than PV03 with respect to the detachment fault (Figure 3). The high-aluminum hornblende generation in PV03 crystallized in an early stage of the intrusion probably at greater depth. This may be explained with the contemporaneity of VBQD intrusion and ductile extensional shearing as indicated by the structural overprinting relations.

5.3. Tectonic Evolution

Based on the overprinting relations (Figure 7) and the dating results, the following tectonic evolution can be reconstructed: The VBQD intruded in several pulses around ~289 Ma, contemporaneous with D2 mylonitic shearing and D3 folding. The VSBG intruded soon after this (~287 Ma). The VSBG was intruded at shallower depth, as suggested by granophyric structures (Gaetani et al., 2012), probably while the VBQD was being exhumed. Hornblende barometry suggests that the VBQD was exhumed by ~5.5 to ~6.5 km after its intrusion, by extensional unroofing along the brittle Grassi Detachment Fault. It follows that the basement was exhumed while D2 mylonitic shearing, D3 folding, and brittle detachment faulting took place. This is an additional supporting evidence for the assumption that D2 top-to-the-Southeast shearing is extensional (Froitzheim et al., 2008), leading to unroofing of the basement.

Although D2 mylonites, D3 folds, intrusions, and brittle deformation along the Grassi Detachment overprint each other, they are all compatible with a framework of NW-SE stretching and unroofing. In fact, these are typical elements of the evolution of extensional metamorphic core complexes. Extension-parallel upright folds, termed corrugation folds or mega-mullions, are typical for large extensional detachments, for example, metamorphic core complexes in western North America (Chemehuevi Mountains; John, 1987; Whipple Mountains, Davis & Lister, 1988), but also for detachment faults of oceanic core complexes at the Mid-Atlantic Ridge (Blackman et al., 1998; Tucholke et al., 1998, 2008). According to Singleton (2013), they result from the reduction of vertical stress during tectonic unroofing. Core-complex formation, including D2, D3, and the brittle Grassi Detachment, took place while the Collio Formation was deposited.

5.4. Reconstruction of the Permian Metamorphic Core Complex

The geometry of the Permian metamorphic core complex is difficult to reconstruct because, on one hand, it was partly eroded before the Late Permian and, on the other hand, it was slightly folded by the Orobic Anticline in the framework of Alpine thrusting. However, the field structural relations suggest that the culmination of the core complex was located between the cutoff line of the Ponteranica Conglomerate and the Sasso Rosso Fault, as discussed in the following.

The angular unconformity at the base of the Verrucano Lombardo may be explained by erosion of topography created by Early Permian detachment faulting. The erosional cutoff points of the Ponteranica Conglomerate, on the northern flank of the Orobic Anticline (close to Val Biandino; Figure 3) and on the southern flank (SW of Primaluna), define a SW-NE cutoff line crossing the valley a short distance east of Primaluna. The topographic culmination of the core complex must have been located northwest of this line. The Sasso Rosso Fault, conversely, belongs already to the other flank of the core complex, the updip flank

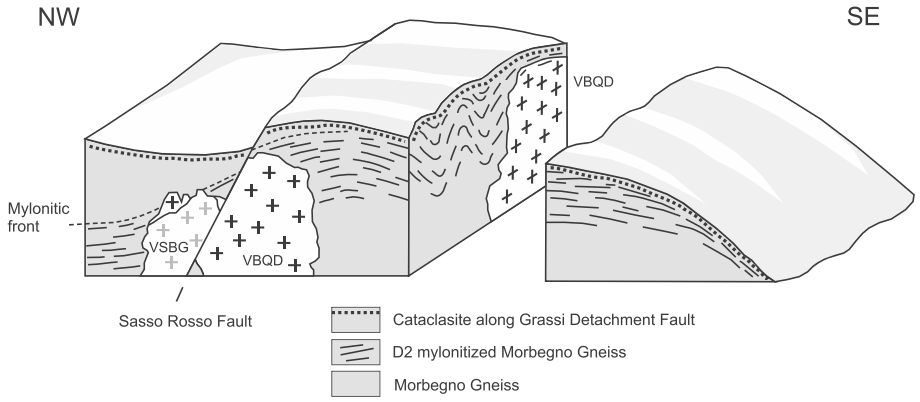

Figure 10. Reconstruction of the Early Permian metamorphic core complex in the western Orobic Alps. Only the footwall is shown. The brittle Grassi Detachment Fault was rooted in a ductile mylonite zone. Detachment faulting exhumed the mylonites in a domal antiform; mylonites show corrugation folds parallel to the extension direction. The Sasso Rosso Fault is an antithetic fault supporting the exhumation of the core complex and displacing the mylonitic front. VBQD = Val Biandino Quartz Diorite, VSBG = Valle San Biagio Granite.

with respect to the detachment fault (Figure 10). It was active as a high-angle (~70°), northwest-dipping normal fault antithetic to the Grassi Detachment, toward the end of core complex formation but still before ~260 Ma (see section 5.1). Southeast of the Sasso Rosso Fault, the Morbegno Gneiss is mylonitized, D2 foliation is deformed by upright, extension-direction-parallel corrugation folds (Figure 4, profile C-C′), and stretching lineation is northwest-southeast oriented (Figure 3). In contrast, in the hanging wall of the Sasso Rosso Fault, the structures of the Morbegno Gneiss belong to D1, and D2 mylonites are not found (Figures 3 and 4, profile A-A′). This suggests that the D2 mylonites were downthrown toward the northwest by the Sasso Rosso Fault (Figure 10), as observed for antithetic normal faults along the mylonitic front in Cordilleran metamorphic core complexes (Chéry, 2001; Davis, 1988; Davis & Lister, 1988; Reynolds & Lister, 1990; Spencer & Reynolds, 1986) and, for example, also in the Saxonian Granulite Massif, a Variscan metamorphic core complex in Central Europe (Reinhardt & Kleemann, 1994). Such antithetic normal faults form during a late stage of detachment faulting and accommodate part of the uplift of the core complex (Chéry, 2001; Reynolds & Lister, 1990). Therefore, they are generally located on the updip side of the core complex. We suggest that the metamorphic core complex comprised approximately the area of the map in Figure 3 and culminated close to Primaluna.

5.5. Early Permian Tectonic Framework and Implications for the Pangea A Versus B Controversy

To assess the Early Permian tectonic framework in the Southern Alps, post-Early-Permian rotation of the Southern Alps has to be taken into account. Muttoni et al. (2003) determined paleomagnetic directions of Early Permian volcanic rocks in the Southern Alps, both in the Athesian Volcanic Province and in the Lugano-Valganna area (Figure 2), that is, east and west of our study area. Paleomagnetic declinations, corrected for bed tilting, are between 139.4° and 160.4°E, with a mean of 151.5°E. (cf. Figure 4 in Muttoni et al., 2003). Therefore, the present-day structures have to be rotated ~30° clockwise to restore for the bulk rotation since Early Permian. Some authors, for example, Cassinis et al. (2007), have applied a rotation of 50° to restore the Early Permian paleogeographic situation. This is, however, not correct because 50° is not the Early Permian declination of the Southern Alps but the difference between the Early Permian declinations of stable Europe and the Southern Alps. Applying the 30° rotation, the extension direction of the Grassi Detachment Fault, ~150° in present-day coordinates, results to be N-S in its original, Early Permian orientation (Figure 6d).

The Permian paleofaults in the study area did not act as strike-slip faults but as low- and high-angle normal faults. We did not find evidence for strike-slip faults related to the Collio Basins. However, extensional detachment faults and metamorphic core complexes faults can occur not only in orthogonally extended rifts but also in transtensional situations. An example of the latter is represented by the Turtleback Surfaces on the east side of the Death Valley pull-apart basin (Wright et al., 1974). In Death Valley and other cases, the slip direction of the detachment faults is generally subparallel to the slip direction of the strike-slip faults to which the pull-apart basin is linked (Mancktelow & Pavlis, 1994). Dextral transtension in a WSW-ENE strike-slip fault

zone should then lead to detachment faults with equally WSW-ENE directed slip. The actual extension direction in our study area, N-S in Permian coordinates, differs by ~60° from such an expected slip direction. Therefore, our observations in the Orobic Anticline do not conform with the model that the formation of the Collio Basins and the Early Permian magmatism resulted from the Pangea A to B megashear zone. Even though the Permian continental wrench system has long been regarded as a viable model at regional scale, the local kinematic evidence is inconsistent with diffuse strike-slip faulting and, rather, supports that the Collio Basins and associated magmatism formed in a framework of north-south crustal extension (Marotta & Spalla, 2007; Schuster & Stüwe, 2008; Spalla et al., 2014).

Dextral strike-slip faulting could still have taken place in other regions, or alternatively, during the Middle Permian, after extensional faulting along the Grassi Detachment Fault and before the deposition of the Verrucano Lombardo. The timing of the Pangea B to A transition after Muttoni et al. (2003; ~285–265 Ma) falls partly into this gap. It cannot be excluded that important strike-slip faulting occurred during this time, along so far unidentified faults outside our study area.

5.6. Carboniferous to Permian Magmatism in the Alps

Figure 11 shows a compilation of 209 published U-Pb zircon age determinations of magmatic rocks, both intrusive and volcanic, from the different paleogeographic domains of the Alps. All ages between 350 and 250 Ma, that is, Carboniferous and Permian, were included. Age determinations by other isotopic systems were not included, to produce a homogeneous data set and because U-Pb zircon is a widely applied and reliable method for dating magmatic rocks (supporting information Table S7). The restriction to zircon ages may, however, have led to an underrepresentation of areas where less zircon dating has been performed, in particular the Austroalpine domain (for a compilation of radiometric ages of Permian high-temperature metamorphism, see Kunz et al., 2018).

In the Helvetic, Penninic, and Austroalpine units, the magmatic age distribution is bimodal. An older population, characterized by K- and Mg-rich granitoids (Von Raumer et al., 2013), occurs at 350 to 330 Ma. This roughly coincides with the Variscan collision that took place in the Visean (~348–331 Ma) in the Alpine area (Von Raumer et al., 2013). Consequently, these granitoids represent collisional magmatism. Around 320 Ma, a minimum in magmatic activity is expressed in the age distributions from the Helvetic, Penninic, and Austroalpine domains and in the combined distribution from all domains. A second period of magmatic activity, post-Variscan, follows after this time of relative quiescence. The maximum of this bimodal, often high-K, calcalkaline magmatism shifted in the Alpine area from northwest to southeast. In the Helvetic domain the maximum is at ~310–300 Ma, in the Penninic and Austroalpine domains at ~290 Ma, and in the South Alpine at ~280 Ma. Most of the post-Variscan magmatism predates the paleomagnetic Pangea B to A transformation (~285–265 Ma; Muttoni et al., 2003), suggesting that the magmatism and the hypothetical Pangea B to A transformation are not directly related. Consistently with our data, the post-Variscan magmatism in the Southern Alps occurred in a framework of north-south extension rather than transcurrent shearing.

Also shown in Figure 11 is the time span of dextral transcurrent shearing in the External Massives of the Helvetic Zone. In this part of the Alps, dextral shear zones have been dated by Genier et al. (2008) at ~320 Ma, by Ballèvre et al. (2018) at ~320–310 Ma, and by Simonetti et al. (2018) at ~340–320 Ma. Retrodeformation of Alpine deformation results in an original SW-NE strike for these shear zones. They are interpreted to belong to the dextrally transpressive East Variscan Shear Zone (Corsini & Rolland, 2009). This dextral shearing can obviously not be related to the Pangea B to A transformation because it predates the Early Permian rocks that yielded the paleomagnetic data on which Pangea B is based (Muttoni et al., 2003). Whereas dextral shearing during the Carboniferous at ~340–320 Ma is well documented (e.g., Ballèvre et al., 2018), we found no documentation of fault-rock kinematics of Permian dextral strike-slip faults in the Alps. The only exception is the Cossato-Mergozzo-Brissago in the westernmost Southern Alps, which is, however, controversial (dextral according to Boriani et al., 2016; sinistral according to Handy et al., 1999, and Handy & Streit, 1999). Hence, undisputed evidence for Permian-age dextral shearing is not only missing in our limited study area but generally in the Alps.

The tectonic framework of Early Permian north-south crustal extension in the Alps is not clear. One possibility is gravity-driven extensional collapse of thickened orogenic crust (Dewey, 1988). This process reduces the

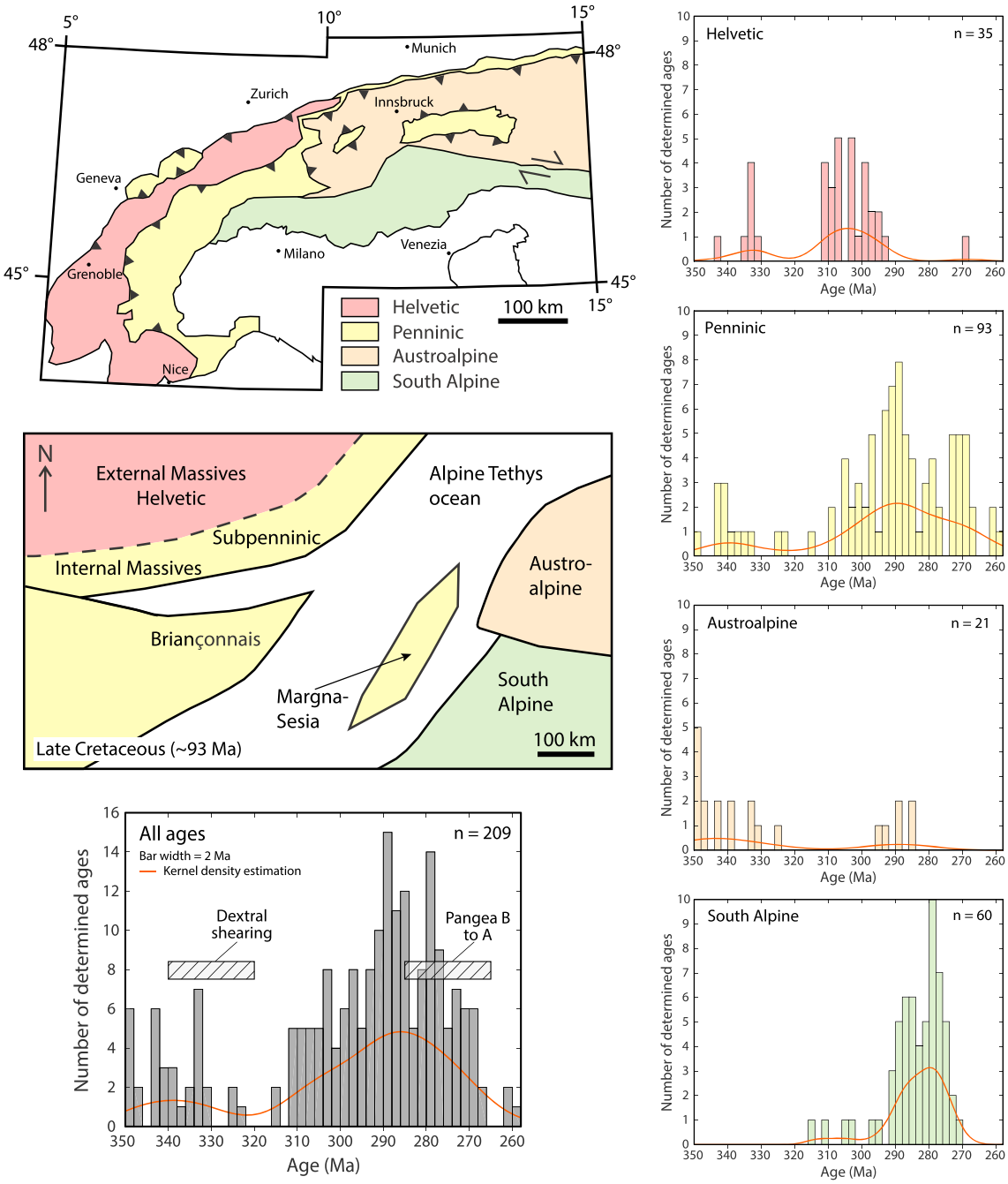

Figure 11. Frequency distribution of U-Pb zircon ages of 209 plutonic and volcanic rocks in the Alps. Present-day map (upper left) shows distribution of tectonic superunits in the Alps, and paleogeographic map (middle left) shows their arrangement in the Late Cretaceous after Liati et al. (2005, modified). *Dextral shearing* in the diagram for all ages (lower left) indicates age range of dextral shear zones in the Helvetic External Massives after Genier et al. (2008) and Simonetti et al. (2018); Pangea B to A indicates age range of transformation from Pangea B to Pangea A after Muttoni et al. (2003). Sources of U-Pb zircon ages: Beltrando et al. (2007); Bergomi et al. (2007, 2017); Berra et al. (2015); Bertrand et al. (1998, 2005); Bossart et al. (1986); Bussien Grosjean et al. (2017); Bussien et al. (2008, 2011); Bussy and Cadoppi (1996); Bussy et al. (1996, 1998, 2000); Capuzzo and Bussy (2000); Cavargna-Sani et al. (2014); Dallagiovanna et al. (2009); Debon et al. (1994); Eichhorn et al. (1999, 2000); Galli et al. (2012); Gretter et al. (2013); Guerrot and Debon (2000); Hansmann et al. (2001); Kebede et al. (2005); Klötzli et al., 2014); Letsch et al. (2015); Liati and Gebauer (2003); Liati et al. (2001); Maino et al. (2012); Mandl et al. (2017); Manzotti et al. (2018); Marocchi et al. (2008); Marquer et al. (1998); Masson et al. (2008); Monjoie et al. (2007); Paquette et al. (1989); Pawlig (2001); Peressini et al. (2007); Petri et al. (2017); quick et al. (2009); Ring et al. (2005); Rubatto et al. (2001); Schaltegger (1993); Schaltegger and Brack (2007); Schaltegger and Corfu (1992, 1995); Sergeev et al. (1995); Veselá et al. (2008, 2011); Visonà et al. (2007); Von Quadt et al. (1994). See supporting information Table S7 for details.

elevation of orogens over the surrounding lowlands and the thickness of the crustal root until the remaining gradient in gravitational potential energy between mountains and lowlands is supported by the strength of the crust. The long time span between collision (348–331 Ma; Von Raumer et al., 2013) and Permian magmatism and Early Permian extension (culminating at ~290 Ma) rather speaks against gravitational collapse (Marotta & Spalla, 2007). The marine ingression in the youngest part of the Collio Formation (Sciunnach, 2001c) also requires a mechanism other than gravitational collapse, since gravitational collapse lowers the elevation of orogens but is unlikely to produce subsidence to sea level. Therefore, a far-field extensional stress component in addition to the regional gravitational stresses is necessary to explain Early Permian extension.

Schuster and Stüwe (2008) assumed extension ahead of the westward-propagating opening of Neotethys. However, most reconstructions imply that this oceanic opening propagated toward NNW, not W (e.g., Muttoni et al., 2009; see Figure 1). Moreover, Latest Carboniferous to Early Permian rifting and geochemically similar high-K, calcalkaline magmatism affected large areas of Central Europe also hundreds of kilometers north of the Alps (e.g., Saar-Nahe basin in Western Germany; Schmidberger & Hegner, 1999). Early Permian rifting, but associated with mildly alkaline magmatism, is also documented for Oslo Graben in southern Norway (Heeremans et al., 1996). Far-field stresses are therefore more likely than a local cause like rift propagation.

6. Conclusions

An Early Permian detachment fault and metamorphic core complex are reconstructed in the Orobic Anticline of the Southern Alps. Elements of this tectonic system are (1) mylonites with NW-SE stretching lineation and top-to-the-Southeast shear sense, developed under decreasing temperature; (2) upright, extension-parallel corrugation folds; (3) a cataclasite layer, the Grassi Detachment Fault, along the basement-cover contact; (4) an antithetic high-angle normal fault on the updip side of the core complex; (5) syntectonic intrusions of quartz diorite and granite in the core complex; and (6) core-complex topography reflected by the erosional unconformity at the base of the Verrucano Lombardo Formation.

The VBQD and the VSBG intruded into the core complex at ~289 to 287 Ma based on U-Pb dating of zircon, contemporaneously with ages reported in the literature for the eruption of volcanic rocks now found in the hanging wall (Monte Cabianca Volcanite of the Collio Formation).

The extension direction, ~150° in present-day coordinates, is restored to N-S when the post-Early-Permian bulk rotation of the Southern Alps is taken into account. Therefore, the situation in the study area does not support pull-apart tectonics related to the WSW-ENE Pangea B to A megashear.

Transpressive, dextral shear zones do occur in the external (Helvetic) part of the Alps, but these are Carboniferous in age and therefore unrelated to the Early Permian basin formation and all the more unrelated to the Middle Permian Pangea B to A transformation. More information about Permian tectonics may be found in other parts of the Southern and Eastern Alps, which eventually will allow a comprehensive reconstruction of the processes leading from the Variscan collision to the opening of Alpine Tethys.

Acknowledgments
The authors thank Niels Jung for thin section preparation. Field work of Florian Pohl was supported by a DAAD Promos scholarship. Florian Pohl thanks Nadine Conze for help and support in the field. All the data used are listed in the references and given in the supporting information. We thank Peter Brack, Michel Ballèvre, Michel Corsini, and an anonymous reviewer for providing constructive reviews that helped to improve the manuscript. Two anonymous reviewers are thanked for their comments on an earlier version of this manuscript.

References

Arthaud, F., & Matte, P. (1977). Late Paleozoic strike-slip faulting in southern Europe and northern Africa: Result of a right-lateral shear zone between the Appalachians and the Urals. *Geological Society of America Bulletin*, *88*(9), 1305–1320. https://doi.org/10.1130/0016-7606(1977)88<1305:LPSFIS>2.0.CO;2

Bakos, F., Del Moro, A., & Visonà, D. (1990). The Hercynian volcanoplutonic association of Ganna (Lake Lugano, central Southern Alps, Italy). *European Journal of Mineralogy*, *2*(3), 373–384. https://doi.org/10.1127/ejm/2/3/0373

Ballèvre, M., Manzotti, P., & Dal Piaz, G. V. (2018). Pre-Alpine (Variscan) inheritance: A key for the location of the future Valaisan basin (Western Alps). *Tectonics*, *37*, 786–817. https://doi.org/10.1002/2017TC004633

Bargossi, G. M., Rottura, A., Vernia, L., Visonà, D., & Tranne, C. A. (1998). Guida all'escursione sul distretto vulcanico atesino e sulle plutoniti di Bressanone-Chiusa e Cima d'Asta. *Memorie della Societa Geologica Italiana*, *53*, 23–41.

Beltrando, M., Rubatto, D., Compagnoni, R., & Lister, G. (2007). Was the Valaisan Basin floored by oceanic crust? Evidence of Permian magmatism in the Versoyen Unit (Valais domain, NW Alps). *Ofioliti*, *32*, 85–99.

Beltrando, M., Stockli, D. F., Decarlis, A., & Manatschal, G. (2015). A crustal-scale view at rift localization along the fossil Adriatic margin of the Alpine Tethys preserved in NW Italy. *Tectonics*, *34*, 1927–1951. https://doi.org/10.1002/2015TC003973

Bergomi, M. A., Dal Piaz, G. V., Malusà, M. G., Monopoli, B., & Tunesi, A. (2017). The grand St Bernard - Briançonnais nappe system and the Paleozoic inheritance of the Western Alps unravelled by zircon U-Pb dating. *Tectonics*, *36*, 2950–2972. https://doi.org/10.1002/2017TC004621

Bergomi, M. A., Tunesi, A., Shi, Y. -R., Colombo, A., & Liu, D. -Y. (2007). SHRIMP II U/Pb geochronological constraints of pre-Alpine magmatism in the lower Penninic units of the Ossola Valley (Western Alps, Italy). *Geophysical Research Abstracts*, *9*, 07780.

Berra, F., Felletti, F., & Tessarollo, A. (2016). Stratigraphic architecture of a transtensional continental basin in low-latitude semiarid conditions: The Permian succession of the central Orobic Basin (Southern Alps, Italy). *Journal of Sedimentary Research*, *86*(4), 408–429. https://doi.org/10.2110/jsr.2016.26

Berra, F., Tiepolo, M., Caironi, V., & Siletto, G. B. (2015). U-Pb zircon geochronology of volcanic deposits from the Permian basin of the Orobic Alps (Southern Alps, Lombardy): Chronostratigraphic and geological implications. *Geological Magazine*, *152*(03), 429–443. https://doi.org/10.1017/S0016756814000405

Bertotti, G. (1991). Early Mesozoic extension and Alpine shortening in the western Southern Alps: The geology of the area between Lugano and Menaggio (Lombardy, northern Italy). *Memorie di Scienze Geologiche dell'Università di Padova*, *43*, 17–123.

Bertrand, J.-M., Guillot, F., Leterrier, J., Perruchot, M. P., Allières, L., & Macaudière, J. (1998). Granitoides de la zone houillère briançonnaise en Savoie et en Val d'Aoste (Alpes occidentales): géologie et géochronologie U-Pb sur zircon. *Geodinamica Acta*, *11*, 33–49.

Bertrand, J.-M., Paquette, J. -L., & Guillot, F. (2005). Permian zircon U-Pb ages in the Gran Paradiso massif: Revisiting post-Variscan events in the Western Alps. *Schweizerische Mineralogische und Petrographische Mitteilungen*, *85*, 15–29.

Blackman, D. K., Cann, J. R., Janssen, B., & Smith, D. K. (1998). Origin of extensional core complexes: Evidence from the Mid-Atlantic Ridge at Atlantis fracture zone. *Journal of Geophysical Research*, *103*(B9), 21315–21333. https://doi.org/10.1029/98JB01756

Blom, J. C., & Passchier, C. W. (1997). Structures along the Orobic thrust, central Orobic Alps, Italy. *Geologische Rundschau*, *86*(3), 627–636. https://doi.org/10.1007/s005310050168

Boriani, A., & Bini, A. (2012). Note illustrative della Carta Geologica d'Italia alla (Foglio 056 'SONDRIO', scala: 1:50.000). IstitutoSuperiore per la Protezione e la Ricerca Ambientale and Regione Lombardia, Servizio Geologico d'Italia, Roma.

Boriani, A., Caironi, V., & Sacchi, R. (2016). The CMB line: The southern margin of the Ivrea-Verbano Zone (basement of the Southern Alps, Italy): A re-appraisal. *Rendiconti Lincei. Scienze Fisiche e Naturali*, *27*(4), 673–678. https://doi.org/10.1007/s12210-016-0548-0

Boriani, A., Colombo, A., & Macera, P. (1985). Radiometric geochronology of Central Alps. *Rendiconti della Societa Italiana di Mineralogia e Petrologia*, *40*, 139–186.

Borsi, S., D'Amico, C., & Del Moro, A. (1974). Studio radiometrico delle rocce intrusive del massiccio di Cima d'Asta (Trentino). *Memorie della Societa Geologica Italiana*, *13*, 145–159.

Bossart, P. J., Meier, M., Oberli, F., & Steiger, H. R. (1986). Morphology versus UPb systematics in zircon: A high-resolution isotopic study of a zircon population from a Variscan dike in the Central Alps. *Earth and Planetary Science Letters*, *78*(4), 339–354. https://doi.org/10.1016/0012-821X(86)90002-6

Bussien, D., Bussy, F., Magna, T., & Masson, H. (2011). Timing of Palaeozoic magmatism in the Maggia and Sambuco nappes and paleogeographic implications (central Lepontine Alps). *Swiss Journal of Geosciences*, *104*(1), 1–29. https://doi.org/10.1007/s00015-010-0049-6

Bussien, D., Bussy, F., Masson, H., Magna, T., & Rodionov, N. (2008). Variscan lamprophyres in the Lower Penninic domain (Central Alps): Age and tectonic significance. *Bulletin de la Société géologique de France*, *179*(4), 369–381. https://doi.org/10.2113/gssgfbull.179.4.369

Bussien Grosjean, D. B., Meisser, N., May-Leresche, S., Ulianov, A., & Vonlanthen, P. (2017). The Morcles microgranite (Aiguilles Rouges, Swiss Alps): Geochronological and geochemical evidences for a common origin with the Vallorcine intrusion. *Swiss Journal of Geosciences*, 1–15.

Bussy, F., & Cadoppi, P. (1996). U-Pb zircon dating of granitoids from the Dora-Maira massif (western Italian Alps). *Schweizerische Mineralogische und Petrographische Mitteilungen*, *76*, 217–233.

Bussy, F., Hernandez, J., & Von Raumer, J. (2000). Bimodal magmatism as a consequence of the post-collisional readjustment of the thickened Variscan continental lithosphere (Aiguilles Rouges-Mont Blanc Massifs, Western Alps). *Transactions of the Royal Society of Edinburgh: Earth Sciences*, *91*(1-2), 221–233. https://doi.org/10.1017/S0263593300007392

Bussy, F., Sartori, M., & Thélin, P. (1996). U-Pb zircon dating in the middle Penninic basement of the Western Alps (Valais, Switzerland). *Schweizerische Mineralogische und Petrographische Mitteilungen*, *76*, 81–84.

Bussy, F., Venturini, G., & Hunziker, J. (1998). U-Pb ages of magmatic rocks of the western Austroalpine Dent-Blanche-Sesia Unit. *Schweizerische Mineralogische und Petrographische Mitteilungen*, *78*, 163–168.

Cadel, G. (1986). Geology and uranium mineralization of the Collio basin (central Southern Alps, Italy). *Uranium*, *2*, 215–240.

Cadel, G., Cosi, M., Pennacchioni, G., & Spalla, M. I. (1996). A new map of the Permo-Carboniferous cover and Variscan metamorphic basement in the central Orobic Alps, Southern Alps-Italy: Structural and stratigraphical data. *Memorie di Scienze Geologiche dell'Università di Padova*, *48*, 1–53.

Capuzzo, N., & Bussy, F. (2000). High-precision dating and origin of synsedimentary volcanism in the Late Carboniferous Salvan-Dorénaz basin (Aiguilles-Rouges Massif, Western Alps). *Schweizerische Mineralogische und Petrographische Mitteilungen*, *80*, 147–167.

Casati, P., & Gnaccolini, M. (1967). Geologia delle Alpi Orobie occidentali. *Rivista Italiana di Paleontologia e Stratigrafia*, *73*, 25–162.

Cassinis, G., Cortesogno, L., Gaggero, L., Perotti, C., & Ronchi, A. (2007). Volcanic products from the Early Permian Collio Basin (Southern Alps) and their geodynamic implications. *Periodico di Mineralogia*, *76*, 25–47. https://doi.org/10.2451/2007PM0007

Cassinis, G., Perotti, C. R., & Ronchi, A. (2012). Permian continental basins in the Southern Alps (Italy) and peri-Mediterranean correlations. *International Journal of Earth Sciences*, *101*(1), 129–157. https://doi.org/10.1007/s00531-011-0642-6

Cavargna-Sani, M., Epard, J. -L., Bussy, F., & Ulianov, A. (2014). Basement lithostratigraphy of the Adula nappe: Implications for Palaeozoic evolution and Alpine kinematics. *International Journal of Earth Sciences*, *103*(1), 61–82. https://doi.org/10.1007/s00531-013-0941-1

Chéry, J. (2001). Core complex mechanics: From the Gulf of Corinth to the Snake Range. *Geology*, *29*(5), 439–442. https://doi.org/10.1130/0091-7613(2001)029<0439:CCMFTG>2.0.CO;2

Corfu, F., Hanchar, J. M., Hoskin, P. W. O., & Kinny, P. (2003). Atlas of zircon textures. *Reviews in Mineralogy and Geochemistry*, *53*(1), 469–500. https://doi.org/10.2113/0530469

Cornelius, H. P. (1916). Zur Kenntnis der Wurzelregion im unteren Veltlin. *Neues Jahrbuch für Mineralogie, Geologie und Paläontologie, Beilage-Band*, *40*, 253–363.

Corsini, M., & Rolland, Y. (2009). Late evolution of the southern European Variscan belt: Exhumation of the lower crust in a context of oblique convergence. *Comptes Rendus Geoscience*, *341*(2-3), 214–223. https://doi.org/10.1016/j.crte.2008.12.002

Dallagiovanna, G., Gaggero, L., Maino, M., Seno, S., & Tiepolo, M. (2009). U-Pb zircon ages for post-Variscan volcanism in the Ligurian Alps (northern Italy). *Journal of the Geological Society, London*, *166*(1), 101–114. https://doi.org/10.1144/0016-76492008-027

Davis, G. A. (1988). Rapid upward transport of mid-crustal mylonitic gneisses in the footwall of a Miocene detachment fault, Whipple Mountains, southeastern California. *Geologische Rundschau*, *77*(1), 191–209. https://doi.org/10.1007/BF01848684

Davis, G. A., & Lister, G. S. (1988). Detachment faulting in continental extension; perspectives from the southwestern US Cordillera. *Geological Society of America Special Papers*, *218*, 133–160. https://doi.org/10.1130/SPE218-p133

De Capitani, L., Delitala, M. C., Liborio, G., Mottana, A., Nicoletti, M., & Petrucciani, C. (1988). K-Ar dating of the val Biandino plutonic complex (Orobic Alps, Italy). *Memorie di Scienze Geologiche dell'Università di Padova*, *40*, 285–294.

De Capitani, L., & Liborio, G. (1988). Trace element abundance in the val Biandino pluton (Southern Alps, Italy). *Memorie di Scienze Geologiche dell'Università di Padova*, *40*, 99–100.
De Sitter, L. U., & De Sitter-Koomans, C. M. (1949). Geology of the Bergamasc Alps, Lombardia, Italy. *Leidse Geologische Mededelingen*, *14*, 1–257.
Debon, F., Cocherie, A., Ménot, R. -P., Vivier, G., & Barféty, J. -C. (1994). Datation du plutonisme magnésien varisque des massifs cristallins externes des Alpes: l'exemple du granite des Sept Laux (massif de Belledonne, France). *Comptes Rendus de l'Académie des Sciences, Paris*, *318*(2), 1497–1504.
Del Moro, A., & Visonà, D. (1982). The epiplutonic Hercynian complex of Bressanone (Brixen, eastern Alps, Italy); Petrologic and radiometric data. *Neues Jahrbuch für Mineralogie (Abhandlungen)*, *145*, 66–85.
Dewey, J. F. (1988). Extensional collapse of orogens. *Tectonics*, *7*(6), 1123–1139. https://doi.org/10.1029/TC007i006p01123
Diella, V., Spalla, M. I., & Tunesi, A. (1992). Contrasting thermomechanical evolutions in the Southalpine metamorphic basement of the Orobic Alps (Central Alps, Italy). *Journal of Metamorphic Geology*, *10*(2), 203–219. https://doi.org/10.1111/j.1525-1314.1992.tb00079.x
Domeier, M., Van der Voo, R., & Torsvik, T. H. (2012). Paleomagnetism and Pangea: The road to reconciliation. *Tectonophysics*, *514-517*, 14–43. https://doi.org/10.1016/j.tecto.2011.10.021
Eichhorn, R., Höll, R., Loth, G., & Kennedy, A. (1999). Implications of U-Pb SHRIMP zircon data on the age and evolution of the Felbertal tungsten deposit (Tauern Window, Austria). *International Journal of Earth Sciences*, *88*(3), 496–512. https://doi.org/10.1007/s005310050281
Eichhorn, R., Loth, G., Höll, R., Finger, F., Schermaier, A., & Kennedy, A. (2000). Multistage Variscan magmatism in the central Tauern Window (Austria) unveiled by U/Pb SHRIMP zircon data. *Contributions to Mineralogy and Petrology*, *139*(4), 418–435. https://doi.org/10.1007/s004100000145
Froitzheim, N., Derks, J. F., Walter, J. M., & Sciunnach, D. (2008). Evolution of an Early Permian extensional detachment fault from synintrusive, mylonitic flow to brittle faulting (Grassi Detachment Fault, Orobic Anticline, Southern Alps, Italy). *Geological Society of London, Special Publication*, *298*(1), 69–82. https://doi.org/10.1144/SP298.4
Gaetani, M., Sciunnach, D., Bini, A., & Rossi, S. (2012). Note illustrative della Carta Geologica d'Italia (Foglio 076 'LECCO', scala: 1:50.000). Instituto Superiore per la Protezione e la Ricerca Ambientale, Servizio Geologico d'Italia, Roma.
Galli, A., Le Bayon, B., Schmidt, M. W., Burg, J. -P., Reusser, E., Sergeev, S. A., & Larianov, A. (2012). U-Pb zircon dating of the Gruf Complex: Disclosing the late Variscan granulitic lower crust of Europe stranded in the Central Alps. *Contributions to Mineralogy and Petrology*, *163*(2), 353–378. https://doi.org/10.1007/s00410-011-0676-6
Gallo, L. C., Tomezzoli, R. N., & Cristallini, E. O. (2017). A pure dipole analysis of the Gondwana apparent polar wander path: Paleogeographic implications in the evolution of Pangea. *Geochemistry, Geophysics, Geosystems*, *18*, 1499–1519. https://doi.org/10.1002/2016GC006692
Genier, F., Bussy, F., Epard, J. -L., & Baumgartner, L. (2008). Water-assisted migmatization of metagraywackes in a Variscan shear zone, Aiguilles-Rouges massif, western Alps. *Lithos*, *102*(3-4), 575–597. https://doi.org/10.1016/j.lithos.2007.07.024
Gretter, N., Ronchi, A., Langone, A., & Perotti, C. R. (2013). The transition between two major Permian tectono-stratigraphic cycles in the central Southern Alps: Results from facies analysis and U/Pb geochronology. *International Journal of Earth Sciences*, *102*(5), 1181–1202. https://doi.org/10.1007/s00531-013-0886-4
Guerrot, C., & Debon, F. (2000). U-Pb zircon dating of two contrasting Late Variscan plutonic suites from the Pelvoux massif (French Western Alps). *Schweizerische Mineralogische und Petrographische Mitteilungen*, *80*, 249–256.
Hammarstrom, J. M., & Zen, E. A. (1986). Aluminum in hornblende: An empirical igneous geobarometer. *American Mineralogist*, *71*(11–12), 1297–1313.
Handy, M. R., Franz, L., Heller, F., Janott, B., & Zurbriggen, R. (1999). Multistage accretion and exhumation of the continental crust (Ivrea crustal section, Italy and Switzerland). *Tectonics*, *18*(6), 1154–1177. https://doi.org/10.1029/1999TC900034
Handy, M. R., & Streit, J. E. (1999). Mechanics and mechanisms of magmatic underplating: Inferences from mafic veins in deep crustal mylonites. *Earth and Planetary Science Letters*, *165*(3-4), 271–286. https://doi.org/10.1016/S0012-821X(98)00272-6
Hansmann, W., Müntener, O., & Hermann, J. (2001). U-Pb zircon geochronology of a tholeiitic intrusion and associated migmatites at a continental crust-mantle transition, Val Malenco, Italy. *Schweizerische Mineralogische und Petrographische Mitteilungen*, *81*, 239–255.
Heeremans, M., Larsen, B. T., & Stel, H. (1996). Paleostress reconstruction from kinematic indicators in the Oslo Graben, southern Norway: New constraints on the mode of rifting. *Tectonophysics*, *266*(1-4), 55–79. https://doi.org/10.1016/S0040-1951(96)00183-7
Irving, E. (1977). Drift of the major continental blocks since the Devonian. *Nature*, *270*(5635), 304–309. https://doi.org/10.1038/270304a0
John, B. E. (1987). Geometry and evolution of a mid-crustal extensional fault system: Chemehuevi Mountains, southeastern California. *Geological Society of London, Special Publication*, *28*(1), 313–335. https://doi.org/10.1144/GSL.SP.1987.028.01.20
Kebede, T., Klötzli, U., Kosler, J., & Skiöld, T. (2005). Understanding the pre-Variscan and Variscan basement components of the central Tauern Window, Eastern Alps (Austria): Constraints from single zircon U-Pb geochronology. *International Journal of Earth Sciences*, *94*(3), 336–353. https://doi.org/10.1007/s00531-005-0487-y
Klötzli, U. S., Sinigoi, S., Quick, J. E., Demarchi, G., Tassinari, C. C. G., Sato, K., & Günes, Z. (2014). Duration of igneous activity in the Sesia magmatic system and implications for high-temperature metamorphism in the Ivrea-Verbano deep crust. *Lithos*, *206-207*, 19–33. https://doi.org/10.1016/j.lithos.2014.07.020
Kunz, B. E., Manzotti, P., von Niederhäusern, B., Engi, M., Darling, J. R., Giuntoli, F., & Lanari, P. (2018). Permian high-temperature metamorphism in the Western Alps (NW Italy). *International Journal of Earth Sciences*, *107*(1), 203–229. https://doi.org/10.1007/s00531-017-1485-6
Laubscher, H. P. (1985). Large-scale, thin-skinned thrusting in the Southern Alps: Kinematic models. *Geological Society of America Bulletin*, *96*(6), 710–718. https://doi.org/10.1130/0016-7606(1985)96<710:LTTITS>2.0.CO;2
Letsch, D., Winkler, W., von Quadt, A., & Gallhofer, D. (2015). The volcano-sedimentary evolution of a post-Variscan intramontane basin in the Swiss Alps (Glarus Verrucano) as revealed by zircon U-Pb age dating and Hf isotope geochemistry. *International Journal of Earth Sciences*, *104*(1), 123–145. https://doi.org/10.1007/s00531-014-1055-0
Liati, A., Froitzheim, N., & Fanning, C. M. (2005). Jurassic ophiolites within the Valais domain of the Western and Central Alps: Geochronological evidence for re-rifting of oceanic crust. *Contributions to Mineralogy and Petrology*, *149*(4), 446–461. https://doi.org/10.1007/s00410-005-0658-7
Liati, A., & Gebauer, D. (2003). Geochronological constraints for the time of metamorphism in the Gruf Complex (Central Alps) and implications for the Adula-Cima Lunga nappe system. *Schweizerische Mineralogische und Petrographische Mitteilungen*, *83*, 159–172.
Liati, A., Gebauer, D., Froitzheim, N., & Fanning, C. M. (2001). U-Pb SHRIMP geochronology of an amphibolitized eclogite and an orthogneiss from the Furgg zone (Western Alps) and implications for its geodynamic evolution. *Schweizerische Mineralogische und Petrographische Mitteilungen*, *81*, 379–393.

Ludwig, K. R. (2012). Isoplot 3.75. A geochronological toolkit for Microsoft Excel. *Berkeley Geochronology Center, Special Publications*, *5*, 1–75.
Ludwig, K. R., & Mundil, R. (2002). Extracting reliable U-Pb ages and errors from complex populations of zircons from Phanerozoic tuffs. *Geochimica et Cosmochimica Acta*, *66*(Supplement 1), 463.
Maino, M., Dallagiovanna, G., Gaggero, L., Seno, S., & Tiepolo, M. (2012). U-Pb zircon geochronological and petrographic constraints on late to post-collisional Variscan magmatism and metamorphism in the Ligurian Alps, Italy. *Geological Journal*, *47*(6), 632–652. https://doi.org/10.1002/gj.2421
Mancktelow, N. S., & Pavlis, T. L. (1994). Fold-fault relationships in low-angle detachment systems. *Tectonics*, *13*(3), 668–685. https://doi.org/10.1029/93TC03489
Mandl, M., Kurz, W., Hauzenberger, C., Fritz, H., Klötzli, U., & Schuster, R. (2017). Pre-Alpine evolution of the Seckau Complex (Austroalpine basement/Eastern Alps): Constraints from in-situ LA-ICP-MS U-Pb zircon geochronology. *Lithos*, *296-299*, 412–430. https://doi.org/10.1016/j.lithos.2017.11.022
Manzotti, P., Rubatto, D., Zucali, M., El Korh, A., Cenki-Tok, B., Ballèvre, M., & Engi, M. (2018). Permian magmatism and metamorphism in the Dent Blanche nappe: Constraints from field observations and geochronology. *Swiss Journal of Geosciences*, *111*(1-2), 79–97. https://doi.org/10.1007/s00015-017-0284-1
Marocchi, M., Morelli, C., Mair, V., Klötzli, U., & Bargossi, G. M. (2008). Evolution of large silicic magma systems: New U-Pb zircon data on the NW Permian Athesian Volcanic Group (Southern Alps, Italy). *The Journal of Geology*, *116*(5), 480–498. https://doi.org/10.1086/590135
Marotta, A. M., & Spalla, M. I. (2007). Permian-Triassic high thermal regime in the Alps: Result of late Variscan collapse or continental rifting? Validation by numerical modeling. *Tectonics*, *26*, TC4016. https://doi.org/10.1029/2006TC002047
Marquer, D., Challandes, N., & Schaltegger, U. (1998). Early Permian magmatism in Briançonnais terranes: The Truzzo granite and Roffna rhyolite (Eastern Penninic nappes, Swiss and Italian Alps). *Schweizerische Mineralogische und Petrographische Mitteilungen*, *78*, 397–414.
Masson, H., Bussy, F., Eichenberger, M., Giroud, N., Meilhac, C., & Presniakov, S. (2008). Early Carboniferous age of the Versoyen ophiolites and consequences: Non-existence of a "Valais Ocean" (Lower Penninic, western Alps). *Bulletin de la Société géologique de France*, *179*(4), 337–355. https://doi.org/10.2113/gssgfbull.179.4.337
Meijers, M. J. M., Hamers, M. F., van Hinsbergen, D. J. J., van der Meer, D. G., Kitchka, A., Langereis, C. G., & Stephenson, R. A. (2010). New Late Paleozoic paleopoles from the Donbas Foldbelt (Ukraine): Implications for the Pangea A vs. B controversy. *Earth and Planetary Science Letters*, *297*(1-2), 18–33. https://doi.org/10.1016/j.epsl.2010.05.028
Merla, G. (1933). Geologia della Valsassina da Introbbio a Bellano. *Memorie di Geologia e Geografia di Giotto Dainelli*, *4*, 1–44.
Milano, P. F., Pennacchioni, G., & Spalla, M. I. (1988). Alpine and pre-Alpine tectonics in the central Orobic Alps (Southern Alps). *Eclogae Geologicae Helvetiae*, *81*, 273–293.
Monjoie, P., Bussy, F., Schaltegger, U., Mulch, A., Lapierre, H., & Pfeifer, H. -R. (2007). Contrasting magma types and timing of intrusion in the Permian layered mafic complex of Mont Collon (Western Alps, Valais, Switzerland): Evidence from U/Pb zircon and 40Ar/39Ar amphibole dating. *Swiss Journal of Geosciences*, *100*(1), 125–135. https://doi.org/10.1007/s00015-007-1210-8
Morel, P., & Irving, E. (1981). Paleomagnetism and the evolution of Pangea. *Journal of Geophysical Research*, *86*(B3), 1858–1872. https://doi.org/10.1029/JB086iB03p01858
Mottana, A., Nicoletti, M., Petrucciani, C., Liborio, G., De Capitani, L., & Bocchio, R. (1985). Pre-Alpine and alpine evolution of the south-alpine basement of the Orobic Alps. *Geologische Rundschau*, *74*(2), 353–366. https://doi.org/10.1007/BF01824902
Mutch, E. J. F., Blundy, J. D., Tattich, B. C., Cooper, F. J., & Brooker, R. A. (2016). An experimental study of amphibole stability in low-pressure granitic magmas and a revised Al-in-hornblende geobarometer. *Contributions to Mineralogy and Petrology*, *171*, 85.1–85.27.
Muttoni, G., Gaetani, M., Kent, D. V., Sciunnach, D., Angiolini, L., Berra, F., et al. (2009). Opening of the Neo-Tethys Ocean and the Pangea B to Pangea A transformation during the Permian. *GeoArabia*, *14*, 17–48.
Muttoni, G., Kent, D. V., & Channell, J. E. T. (1996). Evolution of Pangea: Paleomagnetic constraints from the Southern Alps, Italy. *Earth and Planetary Science Letters*, *140*(1-4), 97–112. https://doi.org/10.1016/0012-821X(96)00038-6
Muttoni, G., Kent, D. V., Garzanti, E., Brack, P., Abrahamsen, N., & Gaetani, M. (2003). Early Permian Pangea 'B' to Late Permian Pangea 'A'. *Earth and Planetary Science Letters*, *215*(3-4), 379–394. https://doi.org/10.1016/S0012-821X(03)00452-7
Nilius, N. P., Froitzheim, N., Nagel, T. J., Tomaschek, F., & Heuser, A. (2016). The Schwarzhorn amphibolite (eastern Rätikon, Austria): An Early Cambrian intrusion in the Lower Austroalpine basement. *Geologica Carpathica*, *67*(2), 121–134. https://doi.org/10.1515/geoca-2016-0008
Paquette, J.-L., Chopin, C., & Peucat, J. -J. (1989). U-Pb zircon, Rb-Sr and Sm-Nd geochronology of high- to very-high-pressure meta-acidic rocks from the western Alps. *Contributions to Mineralogy and Petrology*, *101*(3), 280–289. https://doi.org/10.1007/BF00375313
Pasquaré, G. (1967). Analisi geologico-strutturale del complesso intrusivo di Val Biandino (Alpi Orobie Occidentali). *Memorie della Societa Geologica Italiana*, *6*, 343–357.
Paton, C., Hellstrom, J., Paul, B., Woodhead, J., & Hergt, J. (2011). Iolite: Freeware for the visualisation and processing of mass spectrometric data. *Journal of Analytical Atomic Spectrometry*, *26*(12), 2508–2518. https://doi.org/10.1039/c1ja10172b
Pawlig, S. (2001). Geological evolution of the Monte Rosa: Constraints from geochronology and geochemistry of a talc-kyanite-chloritoid shear zone within the Monte Rosa Granite (Monte Rosa Nappe, Italian Western Alps). (Doctoral dissertation). Retrieved from publications.ub.uni-mainz.de. (https://publications.ub.uni-mainz.de/theses/volltexte/2001/234/pdf/234.pdf). Mainz, Germany: Johannes Gutenberg-Universität.
Peressini, G., Quick, J. E., Sinigoi, S., Hofmann, A. W., & Fanning, M. (2007). Duration of a large mafic intrusion and heat transfer in the lower crust: A SHRIMP U-Pb zircon study in the Ivrea-Verbano Zone (Western Alps, Italy). *Journal of Petrology*, *48*(6), 1185–1218. https://doi.org/10.1093/petrology/egm014
Petri, B., Mohn, G., Skrzypek, E., Mateeva, T., Galster, F., & Manatschal, G. (2017). U-Pb geochronology of the Sondalo gabbroic complex (Central Alps) and its position within the Permian post-Variscan extension. *International Journal of Earth Sciences*, *106*(8), 2873–2893. https://doi.org/10.1007/s00531-017-1465-x
Petrus, J. A., & Kamber, B. S. (2012). VizualAge: A novel approach to laser ablation ICP-MS U-Pb geochronology data reduction. *Geostandards and Geoanalytical Research*, *36*(3), 247–270. https://doi.org/10.1111/j.1751-908X.2012.00158.x
Philippe, S., Villemaire, C., Lancelot, J. R., Girod, M., & Mercadier, H. (1987). Données minéralogiques et isotopiques sur deux gîtes hydro-thermaux uranifères du bassin volcano-sédimentaire permien de Collio Orobico (Alpes Bergamasques): mise en évidence d'une phase de remobilisation crétacée. *Bulletin de Mineralogie*, *110*, 283–303.
Pin, C. (1986). Datation U-Pb sur zircon á 285 Ma du complexe gabbro dioritique du Val Sesia—Val Mastallone et âge tardi-hercynien du métamorphisme granulitique de la zone Ivrea-Verbano (Italie). *Comptes Rendus de l'Académie des Sciences*, *303*(9), 827–830.
Pinarelli, L., Del Moro, A., & Boriani, A. (1988). Rb-Sr geochronology of Lower Permian plutonism in Massiccio Dei Laghi, Southern Alps (NW Italy). *Rendiconti della Societa Italiana di Mineralogia e Petrologia*, *43*, 411–428.

Porro, C. (1897). Cenni preliminari ad un rilievo geologico nelle Alpi Orobie (Valsassina e Pizzo dei Tre Signori). *Rendiconti Reale Istituto Lombardo di Scienze e Lettere*, *32*, 408–419.
Quick, J. E., Sinigoi, S., Peressini, G., Demarchi, G., Wooden, J. L., & Sbisá, A. (2009). Magmatic plumbing of a large Permian caldera exposed to a depth of 25 km. *Geology*, *37*(7), 603–606. https://doi.org/10.1130/G30003A.1
Real, C., Froitzheim, N., Carosi, R., & Ferrando, S. (2018). Evidence of large-scale Mesozoic detachments preserved in the basement of the Southern Alps (northern Lago di Como area). *Italian Journal of Geosciences*, *137*(2), 283–293. https://doi.org/10.3301/IJG.2018.15
Reinhardt, J., & Kleemann, U. (1994). Extensional unroofing of granulitic lower crust and related low-pressure, high-temperature metamorphism in the Saxonian Granulite Massif, Germany. *Tectonophysics*, *238*(1-4), 71–94. https://doi.org/10.1016/0040-1951(94)90050-7
Reynolds, S. J., & Lister, G. S. (1990). Folding of mylonitic zones in Cordilleran metamorphic core complexes: Evidence from near the mylonitic front. *Geology*, *18*(3), 216–219. https://doi.org/10.1130/0091-7613(1990)018<0216:FOMZIC>2.3.CO;2
Ring, U., Collins, A. S., & Kassem, O. K. (2005). U-Pb SHRIMP data on the crystallization age of the Gran Paradiso augengneiss, Italian Western Alps: Further evidence for Permian magmatic activity in the Alps during break-up of Pangea. *Swiss Journal of Geosciences*, *98*, 363–370.
Rivalenti, G., Rossi, A., Siena, F., & Sinigoi, S. (1984). The layered series of the Ivrea-Verbano igneous complex, western Alps, Italy. *Tschermaks Mineralogische Und Petrographische Mitteilungen*, *33*(2), 77–99. https://doi.org/10.1007/BF01083065
Rubatto, D., Schaltegger, U., Lombardo, B., Colombo, F., & Compagnoni, R. (2001). Complex Paleozoic magmatic and metamorphic evolution in the Argentera Massif (Western Alps) resolved with U-Pb dating. *Schweizerische Mineralogische und Petrographische Mitteilungen*, *81*, 213–228.
Schaltegger, U. (1993). The evolution of the polymetamorphic basement in the Central Alps unravelled by precise U-Pb zircon dating. *Contributions to Mineralogy and Petrology*, *113*(4), 466–478. https://doi.org/10.1007/BF00698316
Schaltegger, U., & Brack, P. (2007). Crustal-scale magmatic systems during intracontinental strike-slip tectonics: U, Pb and Hf isotopic constraints from Permian magmatic rocks of the Southern Alps. *International Journal of Earth Sciences*, *96*(6), 1131–1151. https://doi.org/10.1007/s00531-006-0165-8
Schaltegger, U., & Corfu, F. (1992). The age and source of late Hercynian magmatism in the Central Alps: Evidence from precise U-Pb ages and initial Hf isotopes. *Contributions to Mineralogy and Petrology*, *111*(3), 329–344. https://doi.org/10.1007/BF00311195
Schaltegger, U., & Corfu, F. (1995). Late Variscan "basin and range" magmatism and tectonics in the Central Alps: Evidence from U-Pb geochronology. *Geodinamica Acta*, *8*(2), 82–98. https://doi.org/10.1080/09853111.1995.11105276
Schmidberger, S. S., & Hegner, E. (1999). Geochemistry and isotope systematics of calc-alkaline volcanic rocks from the Saar-Nahe basin (SW Germany)—Implications for Late-Variscan orogenic development. *Contributions to Mineralogy and Petrology*, *135*(4), 373–385. https://doi.org/10.1007/s004100050518
Schmidt, M. W. (1992). Amphibole composition in tonalite as a function of pressure: An experimental calibration of the Al-in-hornblende barometer. *Contributions to Mineralogy and Petrology*, *110*(2–3), 304–310. https://doi.org/10.1007/BF00310745
Schönborn, G. (1990). A kinematic model of the western Bergamasc Alps, Southern Alps, Italy. *Eclogae Geologicae Helvetiae*, *83*, 665–682.
Schönborn, G. (1992). Alpine tectonics and kinematic models of the central Southern Alps. *Memorie - Società Geologica (Padova)*, *44*, 229–393.
Schuster, R., & Stüwe, K. (2008). Permian metamorphic event in the Alps. *Geology*, *36*(8), 603–606. https://doi.org/10.1130/G24703A.1
Sciunnach, D. (2001a). The Lower Permian in the Orobic Anticline (Southern Alps, Lombardy): A review based on new stratigraphic and petrographic data. *Rivista Italiana di Paleontologia e Stratigrafia*, *107*, 47–68.
Sciunnach, D. (2001b). Early Permian palaeofaults at the western boundary of the Collio Basin (Valsassina, Lombardy). *Natura Bresciana*, *25*, 37–43.
Sciunnach, D. (2001c). Benthic formaninifera from the upper Collio Formation (Lower Permian, Lombardy Southern Alps): Implications for the palaeogeography of the peri-Tethyan area. *Terra Nova*, *13*(2), 150–155. https://doi.org/10.1046/j.1365-3121.2001.00339.x
Sciunnach, D. (2003). Fault-controlled stratigraphic architecture and magmatism in the Western Orobic Basin (Lower Permian, Lombardy Southern Alps). *Bollettino della Società Geologica Italiana, Volume speciale*, *2*, 49–58.
Sergeev, S. A., Meier, M., & Steiger, R. H. (1995). Improving the resolution of single-grain U/Pb dating by use of zircon extracted from feldspar: Application to the Variscan magmatic cycle in the Central Alps. *Earth and Planetary Science Letters*, *134*(1-2), 37–51. https://doi.org/10.1016/0012-821X(95)00105-L
Siletto, G. B., Spalla, M. I., Tunesi, A., Lardeaux, J. M., & Colombo, A. (1993). Pre-Alpine structural and metamorphic histories in the Orobic Southern Alps, Italy. In J. F. von Raumer, & F. Neubauer (Eds.), *Pre-Mesozoic geology of the Alps*, (pp. 585–598). Berlin: Springer.
Simonetti, M., Carosi, R., Montomoli, C., Langone, A., D'Addario, E., & Mammoliti, E. (2018). Kinematic and geochronological constraints on shear deformation in the Ferriere-Mollières shear zone (Argentera-Mercantour Massif, Western Alps): Implication for the evolution of the eastern sector of the southern European Variscan Belt. *International Journal of Earth Sciences*, *107*(6), 2163–2189. https://doi.org/10.1007/s00531-018-1593-y
Singleton, J. S. (2013). Development of extension-parallel corrugations in the Buckskin-Rawhide metamorphic core complex, west-central Arizona. *Geological Society of America Bulletin*, *125*(3–4), 453–472. https://doi.org/10.1130/B30672.1
Sláma, J., Košler, J., Condon, D. J., Crowley, J. L., Gerdes, A., Hanchar, J. M., et al. (2008). Plešovice zircon—A new natural reference material for U-Pb and Hf isotopic microanalysis. *Chemical Geology*, *249*, 1–35.
Spalla, M. I., Siletto, G. B., di Paola, S., & Gosso, G. (2000). The role of structural and metamorphic memory in the distinction of tectono-metamorphic units: The basement of the Como lake in the Southern Alps. *Journal of Geodynamics*, *30*(1-2), 191–204. https://doi.org/10.1016/S0264-3707(99)00033-2
Spalla, M. I., Zanoni, D., Marotta, A. M., Rebay, G., Roda, M., Zucali, M., & Gosso, G. (2014). The transition from Variscan collision to continental break-up in the Alps: Insights from the comparison between natural data and numerical model predictions. *Geological Society, London, Special Publications*, *405*(1), 363–400. https://doi.org/10.1144/SP405.11
Spencer, J. E., & Reynolds, S. J. (1986). Some aspects of the middle tertiary tectonics of Arizona and southeastern California. *Arizona Geological Society Digest*, *16*, 102–107.
Stähle, V., Frenzel, G., Hess, J. C., Saupé, F., Schmidt, S. T., & Schneider, W. (2001). Permian metabasalt and Triassic alkaline dykes in the northern Ivrea zone: Clues to the post-Variscan geodynamic evolution of the Southern Alps. *Schweizerische Mineralogische und Petrographische Mitteilungen*, *81*, 1–21.
Thöni, M., Mottana, A., Delitala, M. C., De Capitani, L., & Liborio, G. (1992). The Val Biandino composite pluton: A late Hercynian intrusion into the South-Alpine metamorphic basement of the Alps (Italy). *Neues Jahrbuch für Mineralogie Monatshefte*, *12*, 545–554.
Tucholke, B. E., Behn, M. D., Buck, W. R., & Lin, J. (2008). Role of melt supply in oceanic detachment faulting and formation of megamullions. *Geology*, *36*(6), 455–458. https://doi.org/10.1130/G24639A.1
Tucholke, B. E., Lin, J., & Kleinrock, M. C. (1998). Megamullions and mullion structure defining oceanic metamorphic core complexes on the Mid-Atlantic Ridge. *Journal of Geophysical Research*, *103*(B5), 9857–9866. https://doi.org/10.1029/98JB00167

Van der Voo, R., & Torsvik, T. H. (2001). Evidence for late Paleozoic and Mesozoic non-dipole fields provides an explanation for the Pangea reconstruction problems. *Earth and Planetary Science Letters*, *187*, 71–81.

Veselá, P., Lammerer, B., Wetzel, A., Söllner, F., & Gerdes, A. (2008). Post-Variscan to Early Alpine sedimentary basins in the Tauern Window (wastern Alps). *Geological Society, London, Special Publications*, *298*(1), 83–100. https://doi.org/10.1144/SP298.5

Veselá, P., Söllner, F., Finger, F., & Gerdes, A. (2011). Magmato-sedimentary Carboniferous to Jurassic evolution of the Western Tauern window, eastern Alps (constraints from U-Pb zircon dating and geochemistry). *International Journal of Earth Sciences*, *100*, 993–1027.

Visonà, D., Fioretti, A. M., Poli, M. E., Zanferrari, A., & Fanning, M. (2007). U-Pb SHRIMP zircon dating of andesite from the dolomite area (NE Italy): Geochronological evidence for the early onset of Permian volcanism in the eastern part of the Southern Alps. *Swiss Journal of Geosciences*, *100*(2), 313–324. https://doi.org/10.1007/s00015-007-1219-z

Von Quadt, A., Grünenfelder, M., & Büchi, H. (1994). U-Pb zircon ages from igneous rocks of the Bernina nappe system (Grisons, Switzerland). *Schweizerische Mineralogische und Petrographische Mitteilungen*, *74*, 373–382.

Von Raumer, J. F., Bussy, F., Schaltegger, U., Schulz, B., & Stampfli, G. M. (2013). Pre-Mesozoic Alpine basements—Their place in the European Paleozoic framework. *Geological Society of America Bulletin*, *125*(1-2), 89–108. https://doi.org/10.1130/B30654.1

Voshage, H., Hofmann, A. W., Mazzucchelli, M., Rivalenti, G., Sinigoi, S., & Demarchi, G. (1990). Isotopic evidence from the Ivrea zone for a hybrid lower crust formed by magmatic underplating. *Nature*, *347*, 731–736.

Wiedenbeck, M., Alle, P., Corfu, F., Griffin, W. L., Meier, M., Oberli, F., et al. (1995). Three natural zircon standards for U-Th-Pb, Lu-Hf, trace element and REE analyses. *Geostandards and Geoanalytical Research*, *19*(1), 1–23. https://doi.org/10.1111/j.1751-908X.1995.tb00147.x

Wiedenbeck, M., Hanchar, J. M., Peck, W. H., Sylvester, P., Valley, J., Whitehouse, M., et al. (2004). Further characterisation of the 91500 zircon crystal. *Geostandards and Geoanalytical Research*, *28*(1), 9–39. https://doi.org/10.1111/j.1751-908X.2004.tb01041.x

Wright, L. A., Otton, J. K., & Troxel, B. W. (1974). Turtleback surfaces of Death Valley viewed as phenomena of extensional tectonics. *Geology*, *2*(2), 53–54. https://doi.org/10.1130/0091-7613(1974)2<53:TSODVV>2.0.CO;2

Zanchetta, S., Malusà, M. G., & Zanchi, A. (2015). Precollisional development and Cenozoic evolution of the Southalpine retrobelt (European Alps). *Lithosphere*, *7*, 662–681.